Fuller

OCT 2001

REPORT DOCUMENTATION PAGE

AFRL-SR-BL-TR-01-

0568

1. AGENCY USE ONLY (Leave blank)	2. REPORT DATE	3. REPORT TYPE AND DATES COVERED
	October 19, 2001	Final Report May 1, 2000 - April 30, 2001

4. TITLE AND SUBTITLE
Investigation of a New Class of Disordered Inorganic Materials

5. FUNDING NUMBERS
F49620-00-C-0022

6. AUTHOR(S)
Sankar Sambasivan
Kimberly A. Steiner

7. PERFORMING ORGANIZATION NAME(S) AND ADDRESS(ES)
Applied Thin Films, Inc.
1801 Maple Ave, Suite 5316
Evanston, IL 60201

8. PERFORMING ORGANIZATION REPORT NUMBER

9. SPONSORING / MONITORING AGENCY NAME(S) AND ADDRESS(ES)
USAF, AFMC
Air Force Office of Scientific Research
801 N. Randolph St., Room 732
Arlington, VA 22203-1977

10. SPONSORING / MONITORING AGENCY REPORT NUMBER

11. SUPPLEMENTARY NOTES

12a. DISTRIBUTION / AVAILABILITY STATEMENT
Approved for public release; distribution is unlimited

20011126 104

13. ABSTRACT *(Maximum 200 Words)*

A new class of high temperature metastable oxides (Cerablak™) based on aluminum phosphate composition was investigated under this program. The study included further understanding the sol-gel synthetic procedure, the structural evolution of the material from the precursor state to the calcined form, extensive microstructural and spectroscopic characterization of powders, and development of coatings targeted toward Air Force applications. Evidence collected showed that the thermal stability limit for the material is above 1400°C in air and the stability is enhanced by the amount of excess aluminum present beyond the 1:1 stoichiometric aluminum phosphate composition. While much of the structural details are still unknown, the presence of Al-O-Al bonds in the amorphous network appears to play an important role in extending the metastability. The hypothesis for the extended metastability has been attributed to low mobility of atoms in the amorphous network which resists crystallization. Thin, dense, and pore-free films were easily deposited on various metal, alloy, and ceramic substrates by a simple dip-coating process. The low mobility of oxygen was demonstrated through pronounced evidence of oxidation protection of stainless steel coupons coated with Cerablak™. The study also included synthesis of Cerablak™ in various forms, determination of key properties and investigating its applicability to specific Air Force applications.

14. SUBJECT TERMS			15. NUMBER OF PAGES: 53
			16. PRICE CODE
17. SECURITY CLASSIFICATION OF REPORT: Unclassified	18. SECURITY CLASSIFICATION OF THIS PAGE: Unclassified	19. SECURITY CLASSIFICATION OF ABSTRACT: Unclassified	20. LIMITATION OF ABSTRACT: UL

Applied Thin Films, Inc.

Investigation of a New Class of Disordered Inorganic Materials

Final Report

May 1, 2000 – April 30, 2001

Dr. Sankar Sambasivan
Kimberly Steiner
Applied Thin Films, Inc.
1801 Maple Ave, Suite 5316
Evanston, IL 60201

Contract number: F49620-00-C-0022

Table of Contents

LIST OF FIGURES

Executive Summary

Under a one year AFOSR program, Applied Thin Films, Inc. (ATFI) extended its investigation of a new class of high temperature amorphous materials based on aluminum phosphate compositions. The primary focus of the investigation was to understand the structure and its evolution from a solution-based precursor route. Some effort was also employed to determine its usefulness as a coating, bulk material, or as a fiber for suitable Air Force applications. The synthetic procedure used appears to hold the key to the formation of this metastable material. In this procedure, a mixture is made using a solution of phosphorous pentoxide in ethanol and aluminum nitrate (hydrated form) in ethanol. It is well known that phosphate esters are readily formed upon dissolution of P_2O_5 in ethanol. As the aluminum nitrate is added to the ethanolic solution containing phosphate esters, it appears that molecular complexation between the P and Al species occur that lead to stable P-O-Al based complexes. The primary evidence for this complexation was obtained from the ^{31}P NMR taken from the precursor solution which showed peaks that do not correspond to phosphate esters suggesting a P-O-Al type complex to exist. The nature or the abundance or the stability of these complexes has not been ascertained, but its influence in the product obtained from pyrolysis has been fairly well established. The pyrolyzed product (decomposed and annealed at 1100°C) yields a black powder which is resistant to crystallization. The black color was initially attributed to oxygen vacancies based on preliminary evidence obtained from XPS/ESCA analyses which showed no presence of carbon or nitrogen within the detection limit (<1 weight %). However, recent work performed under a new AFOSR program has provided convincing evidence that the black color is indeed related to residual carbon. Powders annealed to 1100°C typically contain about 5 wt % carbon whereas powders annealed above 1200°C for extended time periods contain less than 1 wt %. In both cases, the powders appear black which led to the tradename "Cerablak".

It was further determined that addition of excess aluminum in the precursor mixture beyond the stoichiometric ratio of 1Al/1P extended the metastability or delayed the crystallization to much higher temperatures or for longer times. Calorimetric work done on the black powders yielded anomalously high solution enthalpies which was later attributed to the presence of carbon. More recent calorimetry work performed on white amorphous powders showed the energetics to be in more reasonable agreement with the observed metastability. Extensive annealing studies were done to analyze the thermal stability of the powders. Both x-ray diffraction (XRD) and transmission electron microscopy (TEM) analyses were performed to monitor the onset of crystallization. All the TEM work done showed that the material consisted of an amorphous matrix consisting of 20% 5-60 nm sized nanocrystallites of aluminum phosphate dispersed uniformly. Powders annealed for over 100 hours at 1300°C still showed nanocrystalline inclusions (60 nm) to be present and stable. XRD results obtained on most powders corroborated well with the TEM analysis and the patterns were mostly amorphous, but with low intensity broad peaks corresponding to the nanocrystallites. Scherrer analysis performed on the broad XRD peaks correlated well with the size of nanocrystallites observed by TEM. Naturally-occurring silicate opals are remarkably similar to the materials studied here. In the silicate opals, nanocrystalline inclusions of silica with

the tridymite, cristobalite, and mixtures of the two phases are present in an amorphous silica matrix. However, their thermal stability is limited to below 1000°C.

Unlike the nanocrystalline amorphous composites obtained in powder form, thin films of Cerablak formed on ceramic fibers remained completely amorphous at 1200°C even after 100 hours. Since the same precursor was used to produce the films and powder, these results suggest that the decomposition behavior is quite different in the two cases. Further work is underway to better understand the interplay between decomposition kinetics and phase formation.

Based on the convincing evidence from the microstructural characterization of the amorphous character, a significant level of effort was employed to study the structure of the material using spectroscopic techniques. Fourier Transform Infra-Red (FTIR), Nuclear Magnetic Resonance (NMR), and Raman Spectroscopic techniques were used to study the various aspects of coordination and bonding of the amorphous network. Collectively, these analyses showed that the network primarily consisted of tetrahedrally coordinated Al-O and P-O polyhedra. In addition, it was determined that a significant fraction of the aluminum was present in octahedral coordination. Based on the FTIR and Raman spectra, it was initially concluded that P=O was present in appreciable amount which seemed logical based on its presence in the precursor as well as it serving as a terminal group for arresting oxygen diffusion. However, it was determined recently that the Raman absorption originally assigned to P=O was actually related to the presence of residual amounts of "graphitic" carbon which absorbs strongly in Raman.

Efforts were also employed to explore the technological significance of this discovery. Providing adequate protection to metal, alloy, and ceramic surfaces from degradation at high temperatures has been a challenging task for a broad range of Air Force and commercial applications. To that end, Cerablak offers an excellent opportunity with a material that is chemically inert with low oxygen permeability and has been determined to be compatible with several metals, alloys, and ceramics at high temperatures. In addition, the alcoholic precursor solution is very suitable to form a continuous film and pyrolyzes favorably to yield a hermetic Cerablak film. Processing techniques to apply thin, hermetic, and pore-free coatings on metal and ceramic substrates were developed. Cerablak coatings developed on steel substrates showed remarkable ability of a 500-1000Å thick coating to protect substrates from oxidation. Cerablak was also formed as fibers from a polymeric precursor and in bulk form by electroconsolidation. Some of the basic physical (hardness, thermal conductivity, thermal expansion, and dielectric constant) and chemical properties (stability in steam and compatibility with other metals and ceramics) were also determined. Over the past year, Cerablak has been tested specifically for protection against molten aluminum, protective coatings on superalloys and bondcoats, as matrix material for ceramic matrix composites suitable for aeroturbines and low observables for Air Force applications, and as oxidation resistant interface coatings for ceramic matrix composites

Much progress was made during this one-year program that extended our understanding of Cerablak's synthesis, structure, properties, and potential applications. Ongoing work under the new 3-year AFOSR program and other federally-funded technology programs will enable

us to gain better insight into the fundamental aspects including the genesis of this new class of materials and also help establish the broad technological relevance anticipated.

Introduction

Applied Thin Films, Inc. (ATFI) is developing a new class of high temperature amorphous materials for a broad range of military and commercial applications. The composition is based on aluminum phosphate where the pseudo-amorphous nature is primarily controlled by atomistic manipulation of a solution-based synthetic route and further stabilized by addition of excess alumina. The powder material derived from pyrolysis of an alcoholic solution of phosphorous pentoxide and aluminum nitrate is black in color which is retained even after annealing in air above 1400°C. Cerablak is the tradename given to the material attributable to the black color. Extensive x-ray diffraction and TEM analysis have provided convincing evidence that the material annealed above 1400°C in air still retains amorphous character greater than 50 volume % along with the presence of isolated nanocrystallites (5-100 nm) of aluminum phosphate randomly distributed throughout the amorphous matrix. Basically, this is a demonstration of power of sol-gel as a synthetic tool to make new and novel materials. Sol-gel techniques offer the ability to tailor the chemistry at the molecular level such that novel materials can be produced with unique properties. Amorphous silicon-based non-oxides (Silicon oxycarbides, oxynitrides, etc.) have been synthesized using polymeric precursors and known to be stable to ultra-high temperatures. This is the first report of an oxide material synthesized using sol-gel precursors which is metastable above 1400°C. While it is suspected that formation of molecular complexes between phosphorous and aluminum species in solution is responsible for the nature of the pyrolyzed product, no convincing evidence have been yet uncovered to prove that hypothesis. However, annealing studies have convincingly proven that addition of excess aluminum (beyond the 1:1 Al/P stoichiometry) extends the metastability to much higher temperatures.

The objective of the one year AFOSR effort was to further understand the nature and behavior of the amorphous material and to study its evolution from the precursor stage. The tasks included synthesis of coatings and bulk materials, investigating its stability under various conditions, determining key properties, and conducting extensive spectroscopic and microstructural characterization to study its molecular structure and amorphous character.

Background

The unique amorphous structure is derived using a simple, low-cost sol-gel precursor [1], composed of an ethanolic solution of P_2O_5 and $Al(NO_3)_3 \cdot 9H_2O$ in special molar ratios, that yields a pyrolyzed product of "glassy" $Al_{1+x}\ PO_{4+3x/2}$. The thermal stability of the amorphous material is primarily controlled by excess aluminum, where x varies from 0.1 to 1.5. Several compositions have been synthesized in amorphous form and shown to be stable for hundreds of hours above 1200°C. Most crystalline materials synthesized using sol-gel routes undergo amorphous to crystalline transition below 1000°C. In this case, thermodynamic equilibration to stable crystalline alumina and $AlPO_4$ phases does not occur until annealing above 1500°C for few hours. Extremely low oxygen diffusivity in the amorphous material, attributed to a special "Al-O-P" cluster, appears to be dominating the sluggish kinetics.

The results obtained thus far clearly suggest that sol-gel synthetic techniques are indeed powerful in yielding novel/metastable materials with unusual properties primarily because of

the ability to control chemistry at the molecular level. Our synthetic procedure is based on a patented alcoholic precursor solution where P_2O_5, hydrated aluminum nitrate, and ethanol are used as raw materials (US patent 6,036,762). The key point is that poly-esterification of P_2O_5 by ethanol and hydrolysis controls the chemistry of clusters in liquid during which time a "special" sequence of molecular events occur (yet unknown) yielding unique spatial coordinations between P, Al, O, and -OH which is preserved through gelation and calcination. Such behavior has been reported for $AlPO_4$ with lower thermal stability [2, 3].

Aluminum phosphate is a well-known inorganic material that has found many uses in catalysts, refractories, composites, phosphate-bonded ceramics, and many others [4-12]. It is a lightweight material (d=2.56 g/cm^3 for berlinite), highly covalent, chemically inert and stable to relatively high temperatures (~ 1500°C). It is chemically compatible with most widely used ceramic materials including silicon carbide, alumina, mullite, and silica over a moderate range of temperatures. It is isostructural with silica and undergoes similar polymorphic transformations (quartz-type, tridymite, and cristobalite) [13-23]. In fact, its use as a high temperature "engineering ceramic" material is limited primarily because of these phase transformations which involve large molar volume changes. The discovery of the pseudo-amorphous phase in the $AlPO_4$ -Al_2O_3"system"stable over a wide range of temperatures (RT to 1400°C) raises the possibility for its use in bulk form as well as coatings for a broad range of low and high temperature applications.

Interest in developing amorphous $AlPO_4$ materials has been in existence from both a technological and an academic perspective. Silica is well known for its glass forming ability where a continuous network of tetrahedrally coordinated Si-O is formed. $AlPO_4$, being isostructural to silica, has been a subject of discussion as to whether a glassy form of $AlPO_4$ can exist [24, 25]. Synthesis of amorphous forms of aluminum phosphate has been attempted with some success, but the thermal stability is limited to 900°C [26]. In the field of catalysis, amorphous forms of thermally stable catalytic supports with high surface area are desired. Sanz et al completed a thorough study of synthesizing various forms of aluminum phosphates with different source materials (nitrates, sulfates, alkoxide etc.) [27]. $AlPO_4$ synthesized using ethylene oxide-based precursor yielded the most thermally stable product, but crystallized above 900°C.

A series of thermal treatments (1100-1500°C) of the powder material synthesized with varying excess alumina content in aluminum phosphate clearly showed that presence of excess alumina does influence and extend the metastability to higher temperatures. The "extended" metastability to very high temperatures is believed to be related to slow diffusion/kinetics which is certainly an exciting prospect, but this also raises the interesting question as to what causes the barrier to diffusion. Evidence for low diffusivity in the material is further substantiated by the persistence to retain black color (or turn slightly gray) even after annealing in air above 1200°C for many tens of hours or at 1400°C in air for several hours suggesting, perhaps, the oxygen diffusivity to be extremely low. Based on this unique behavior, the material was named Cerablak. Within the sensitivity limits, ESCA analysis showed no presence of nitrogen or carbon, again suggesting the black color to be associated with lack of oxygen. (Subsequent studies have shown this result to be an error; the black color is related to the presence of elemental carbon, which persists to very high

temperatures.) It is true that most of the material does turn white when annealed to 1400°C for over 40 hours and the crystallinity does improve as well. However, close examination of the annealed powder shows many particles present in the powder are still distinctly black, raising the possibility that there may be an optimized form of the material which is most resistant to oxygen diffusion.

Figure 1 is a typical XRD pattern obtained from stoichiometric $AlPO_4$ (x=0). The solution was dried and the powder obtained was calcined to 1100°C in air for one hour and is jet black in color. It is immediately evident from the pattern that the material is not fully crystalline and may contain a significant amount of crystalline disorder or amorphous content. Closer examination of the broad peaks reveals the presence of disordered tridymite and cristobalite forms of $AlPO_4$. Further annealing of this material to higher temperatures in air (1100°C, 163hours) does induce significant crystallization as seen in Figure 1b where the tridymite peaks are much better defined. In contrast, Figure 2 shows the XRD pattern of aluminum phosphate synthesized with 0.75 moles of excess aluminum in the precursor solution and annealed under similar conditions. The striking difference between the patterns in Figure 1b and 2b is immediately apparent, viz., the material with excess alumina appears to have retained the "disorder" (the term disorder is used to describe crystalline disorder or amorphous content or combination thereof).

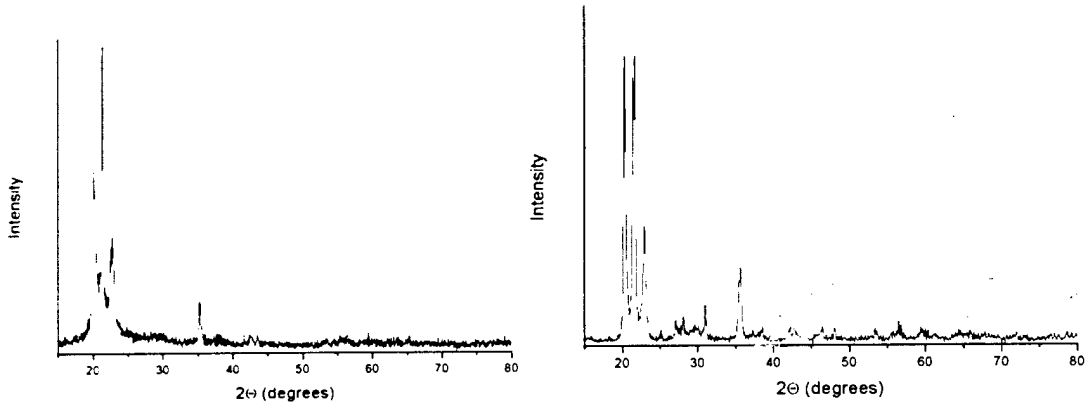

a) b)

Figure 1. XRD pattern for a) Cerablack-1 annealed at 1100°C for 1 hour. b) C-1 annealed at1100°C for 163 hours. Note the splitting of the peak at 21.5, indicating the presence of crystalline tridymite and cristobalite phases.

While the appearance of the amorphous-like pattern for the stoichiometric $AlPO_4$ in Figure 1a was indeed surprising and new, the pattern in Figure 2b with excess alumina was even more intriguing and immediately peaked our interest. The key question, among others, is - why did the excess alumina not crystallize out as corundum upon exposure to very high temperatures? Certainly, there are no known phases of aluminum phosphate with solid solution of alumina [28, 29]. In both cases, the material was black in color with some areas being white.

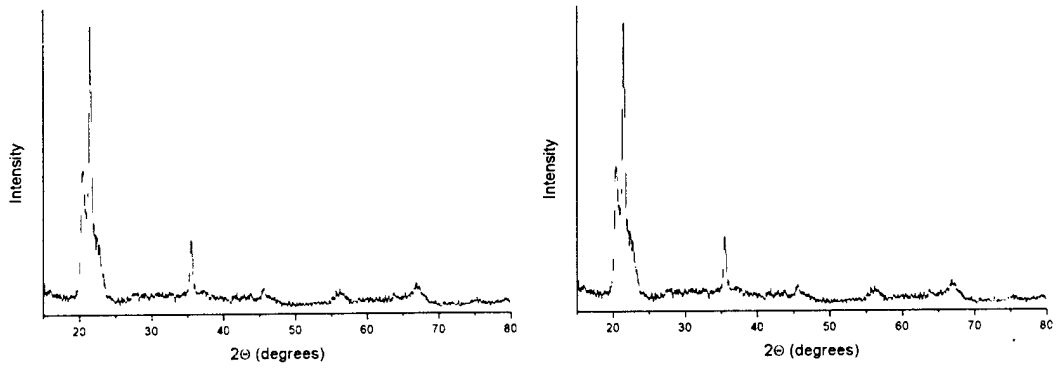

a) b)

Figure 2. XRD 2Θ scanning for C-1.75 annealed to a) 1100°C, 1h b) 1100°C, 163 h. Note the lack of differentiation of the tridymite peaks.

Based on the above results, a series of thermal treatments (over hundred experiments) was done to better understand this phenomenon and evolution of the amorphous-like structure. Excess aluminum content was varied from x=0.1 to 9 and in all cases the enhanced stability of the amorphous matrix was observed. In fact, Cerablak with a Al:P molar ratio of 10:1 was synthesized, and powder annealed to 1100°C for 100 hours showed only low intensity broad peaks corresponding to γ-alumina (Figure 3). Thus, the addition of even small amounts of phosphorous has a tendency to stabilize the amorphous nature. The solid solution range of alumina content in this material is extensive and this can be very useful in designing a functionally graded coating to accommodate thermal mismatch or chemical interference or other factors. For all the studies, the excess alumina content was varied from 0. 25 to 2, but most of the detailed work was done using stoichiometric and C-1.75 samples.

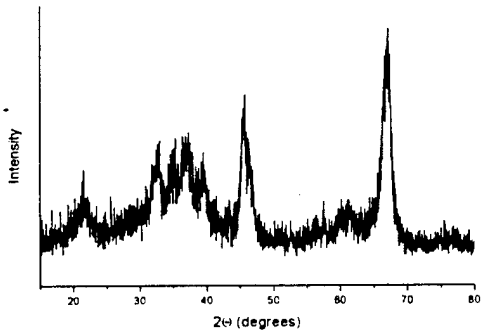

Figure 3. XRD pattern of Cerablak (x=10) annealed to 1100°C for 100 hours. Lines indicate positions of γ-alumina peaks.

While it is certain that the crystallinity of the powders, in general, increased with higher temperature treatments, there is no doubt that significant amount of the powder still appeared amorphous. For powders annealed above 1400°C for over 24 hours, peaks corresponding to small amounts of corundum began to appear in the XRD pattern (see arrow in Figure 4) and

the crystallinity of aluminum phosphate also improved. However, even in samples annealed to 1400°C for over 36 hours, the pattern still contained largely broad peaks suggesting significant amount of amorphous character to be still present. Evidence of the amorphous content was confirmed by TEM analysis as discussed below. Eventually, after annealing at 1600°C, the XRD pattern is a lot sharper and cristobalite phase is seen as the major phase and corundum alumina as the minor phase.

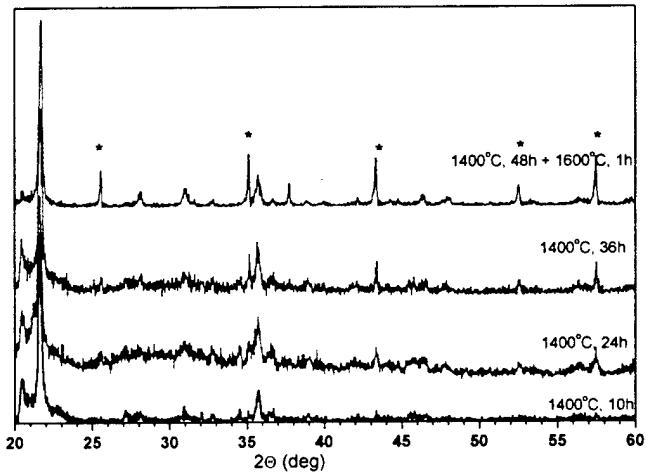

Figure 4. XRD pattern of Cerablak (x=.75) annealed at 1400°C for various times.

NMR spectroscopy gives us some further insight into the structure of Cerablak. Unlike the exclusive tetrahedral coordination for aluminum ions observed in all crystalline polymorphs of $AlPO_4$, ^{27}Al NMR spectra acquired from Cerablak powders show the presence of a broad peak centered near 7-8 ppm along with a prominent peak centered near 39 ppm corresponding to tetrahedral coordination (Fig. 5). The broad feature centered around 8 ppm in the ^{27}Al NMR is assigned to a "distorted" octahedral aluminum (termed octahedral hereafter) which is not known to be present in any crystalline form of $AlPO_4$. The octahedral features, we believe, are solely related to the amorphous content of the material. It is well known that octahedral aluminum species are seen in the gelation stage during synthesis of solution-based aluminum phosphate and that hydroxyl groups are associated with the octahedral aluminum [24, 30, 31]. In most of those cases, upon annealing to above 800-900°C, the octahedral peak intensity decreases due to dehydroxylation and they are converted to tetrahedral aluminums. However, in the case of x=1, the broad octahedral feature persists even after 1400°C anneal for 36 hours. Corundum gives a fairly sharp peak at ~1.8 ppm [27]. The NMR study was done with various compositions of Cerablak (1, 1.5, 2) with annealing done @ 1100°C-163 hours, and 1400°C-36 hours. As Figure 5 shows, the octahedral peak is consistently seen. Although minor changes in peak shape of the octahedral feature changes as α-alumina forms (which contains octahedrally coordinated aluminum). Interestingly, attempts have been made to synthesize aluminophosphate glasses with stoichiometric and excess aluminum using alkoxide-based precursors [24]. However, both compositions resulted in crystalline $AlPO_4$ with no octahedral aluminums present in the calcined material (1000°C).

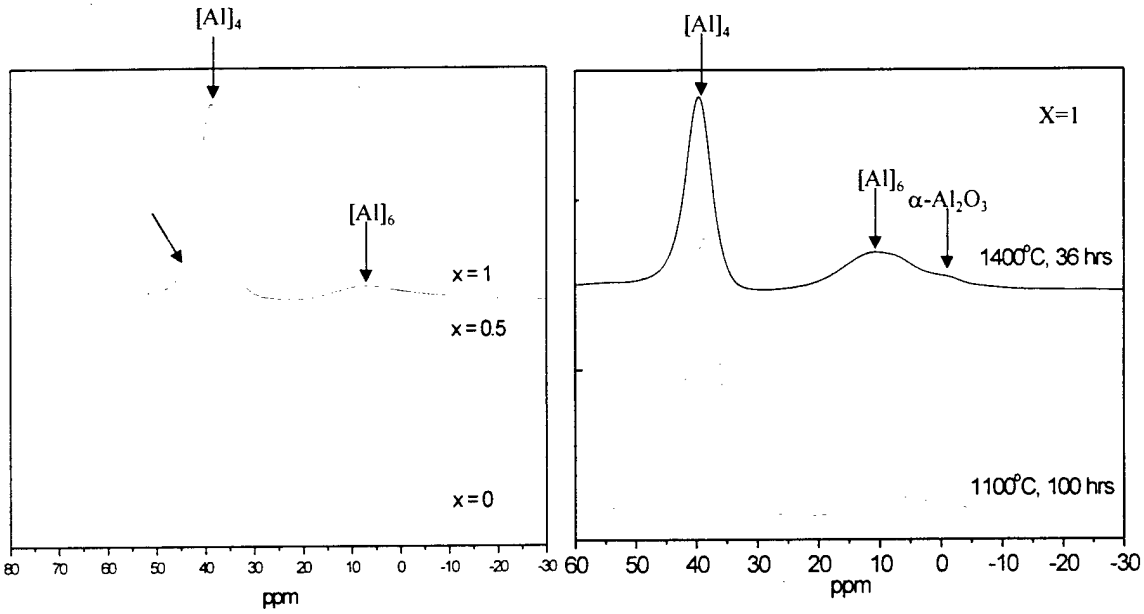

a) b)

Figure 5. ^{27}Al MAS NMR of Cerablak powders. a) Various amounts of excess aluminum after 1100°C, 163hr anneal b) x=1 annealed to 1100°C, 163h and 1400°C, 36h.

In this project, we have explored many aspects of Cerablak, from structural studies by TEM, XRD and vibrational spectroscopy, to determine properties and showing indirect evidence for low oxygen diffusivity.

Results and Discussion

Microstructural Analysis

Extensive XRD and TEM investigation of Cerablak powders and coatings was carried out during this project. X-ray diffraction of most Cerablak powders shows a few low intensity broad peaks, indicating some crystalline content. TEM was used to determine the nature and extent of the crystalline content of Cerablak powders.

Cerablak powders with different thermal histories were examined. Most TEM characterization was performed on powders (x=0.75) annealed under various conditions. The powder samples were prepared by crushing annealed powders in an alumina mortar and pestle. The powders were mixed with acetone or methanol to form a slurry and dropped on to a lacey carbon covered copper grid. No further processing or ion milling was required. A Hitachi HF-2000 high resolution TEM operating at 200kV was used. Energy dispersive x-ray spectroscopy (EDS) was used to confirm elemental composition.

All Cerablak powders examined by TEM showed nanocrystalline inclusions in an amorphous matrix. The size of the nanocrystalline inclusions ranged from 5-80 nm. As the powders were annealed to higher temperatures, the size of the inclusions, and therefore net crystalline content, increased, but even after 1400°C, 10 hour anneal, over ~50% of the material remained amorphous. An extensive library of TEM images and electron diffraction patterns is given in Appendix A.

The first sample imaged was Cerablak (x=0.75) 1100°C, 1hr. This sample contained an amorphous/glassy matrix with nm-sized crystalline inclusions that ranged from 5-30 nm (Figure 6) and were fairly well dispersed. EDS profiles taken from these inclusions showed presence of Al, O, P, but many also showed presence of some impurities including calcium and tungsten, most likely from scheelite ($CaWO_4$) nanocrystals formed because of contamination in the crucible used to anneal powders.

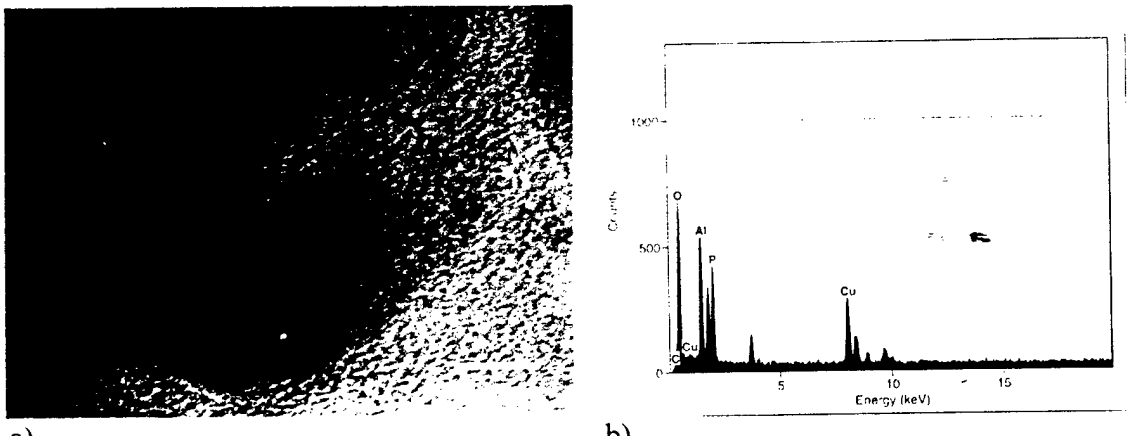

a) b)

Figure 6. TEM study of Cerablak powder (x=0.75) annealed to 1100°C, 1h. a) micrograph showing nanocrystalline inclusion in an amorphous matrix. b) EDS from an inclusion, showing peaks from Ca and W.

Many other thermal treatments of Cerablak have been examined in the TEM (Fig. 7). They include: 1200°C, 420 hr (both x=0 and x=0.75); 1300°C, 100 hr; 1400°C, 10hr (both crushed and uncrushed prior to anneal); 5mol% Er-doped 1100°C, 1 hr; and Cerablak coatings on Nextel 720 fabric after 1200°C, 2 hr and 1200°C, 100 hr anneals. All powder samples show nanocrystalline inclusions in an amorphous matrix, which increase in size with temperature. The crystalline count does not seem to increase with higher temperature anneals, but the crystallite size increases with temperature.

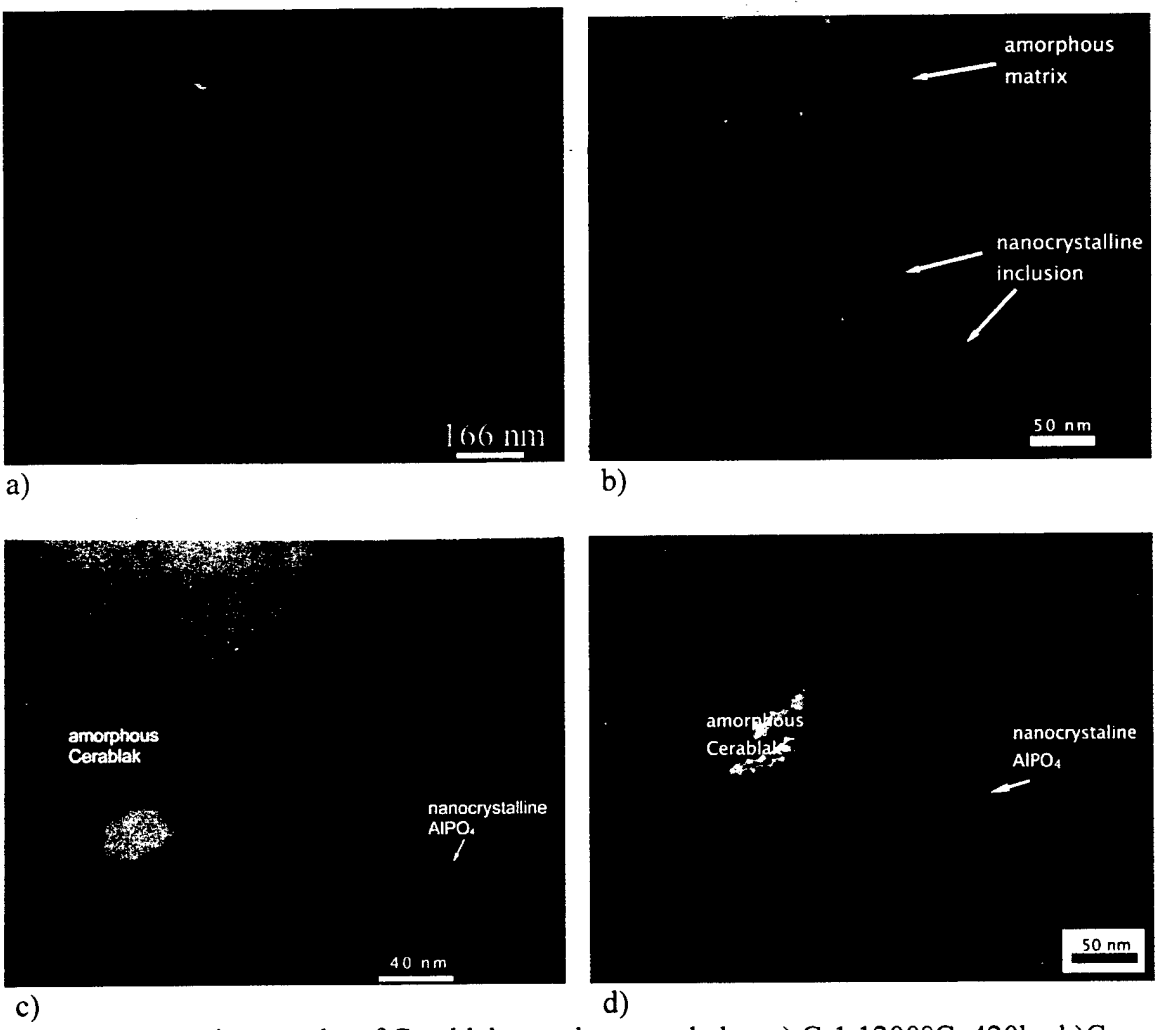

Figure 7. TEM micrographs of Cerablak powder annealed to a) C-1 1200°C, 420h. b)C-1.75, 1200°C, 420h. c) C-1.75 1300°C, 100h d) C-1.75 1400°C, 10h.

TEM examinations of a thin Cerablak film (50-100 nm) after anneal at 1200°C for 2 and 100 hours in air show that the Cerablak remains completely amorphous (Fig. 8). Thin films retain the amorphous character under more extreme conditions than the bulk powder. We attribute the greater degree of amorphous character in the films than powders to the effect of pyrolysis kinetics of the thin film.

attribute the greater degree of amorphous character in the films than powders to the effect of pyrolysis kinetics of the thin film.

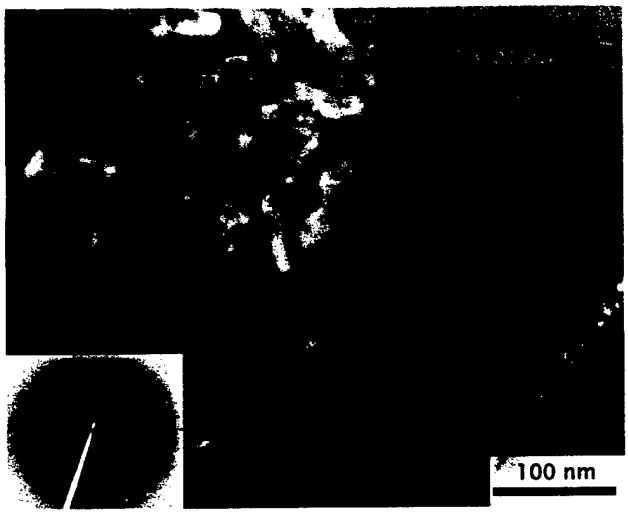

a)

b)

c)

Figure 8. TEM micrographs of a thin Cerablak coating a) annealed 1200°C, 2h. b)fiber-Cerablak coating interface after 1200°C, 2h anneal c) fiber-Cerablak interface after anneal at 1200°C, 100h.

A key probing question in this investigation relates to the compositional range of the amorphous matter. While a range of Al/P ratios in the precursor mixture have been examined, it is still unclear as to the ideal composition of the amorphous matter that provides the maximum thermal stability. As 20-30% of the material is in the form of nanocrystallites, the amorphous matrix in the powder must contain a higher fraction of aluminum than the initial amount in the precursor mixture. The composition of the amorphous matrix can be estimated by determining the crystalline content and assuming that the nanocrystals are stoichiometric (no compositional range in crystalline $AlPO_4$ has ever been reported) and that all of the excess aluminum must therefore be present in the amorphous matrix.

Analysis of diffraction patterns obtained from the nanocrystalline inclusions to confirm the tridymite or cristobalite phase was also not feasible. It is apparent from the XRD that the nanocrystallites represent both the tridymite and cristobalite forms of $AlPO_4$. In addition, the determination of precise camera length of the microscope used requires the use of a diffraction standard. For further discussion on this matter, see below.

Comparison with silicate opal

Cerablak has been shown to be very similar to a particular class of paracrystalline silicate opals having the formula $SiO_2 - nH_2O$ where n is in the range of 0.1 to 0.25 [32, 33]. Water in these silicates is present as bulk silanol groups as well as in molecular form leading to speculation about its possible role in the phosphoaluminate analog.

Silicate opals consist of nanocrystals of SiO_2 embedded in an amorphous hydrated silica matrix. The crystals appear to be anhydrous. These minerals, arising from a low temperature hydrothermal diagenetic process, are generally known as opal-C and opal-CT and are usually partially amorphous with ordered domains consisting of interstratified layers of cristobalite and tridymite with varying degrees of long range order [34]. Diagenesis results in a gradual conversion of tridymite layers to cristobalite with an increase in long range order such that the high angle shoulder disappears and smaller peaks are resolvable, particularly from 41 to 44° 2θ (3,4). Thus, opal-CT is converted into the more highly ordered opal-C. Opal-CT is derived from x- ray amorphous opaline minerals, of which there are several, often referred to as opal-A, opal-AG, or opal-AN [35, 36]. These in turn arise from diatomaceous sediments.

Immediately evident upon examination of the XRD data is a striking similarity between Cerablak and silicate opaline minerals (Fig. 9) [32-38]. The opal analog phases, whether silicate or $AlPO_4$, show only broad features between 19.5° and 24° 2θ as well as a broad line between 35° and 36°. These features correspond to certain intense lines in patterns for the tridymite and cristobalite forms of $AlPO_4$ [39, 40] and SiO_2 [41, 42].

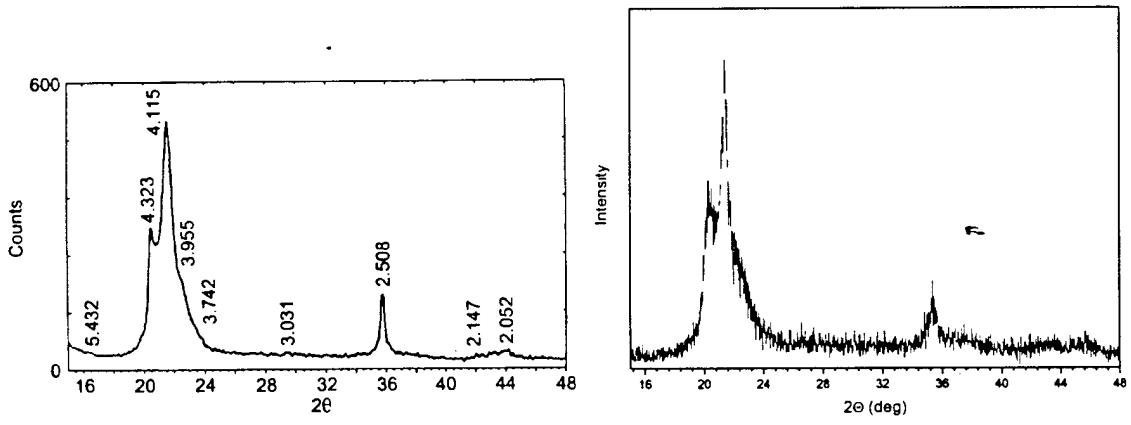

Figure 9. XRD pattern of silicate opal-CT [43] b) XRD pattern of Cerablak (x=0.75)

Opals are identified by their x-ray diffraction patterns, as well as TEM. The various opal polymorphs have characteristic x-ray diffraction patterns. Opal-A forms show only a broad hump centered around 21.5° 2θ. In opal CT, the hump begins to become more intense and to differentiate into 3 peaks. Most opal CT shows one central broad peak, with a shoulder on the left and a barely perceptible shoulder on the right. The x-ray diffraction pattern is similar to both cristobalite and tridymite. Opal C shows primarily the central peak, with small shoulders on either side. Aluminum phosphate tridymite shows three main peaks at 20.305°, 21.499°, and 25.022° 2θ (CuKα radiation). Cristobalite shows one main peak at 21.728° 2θ. As the cristobalite content becomes greater, the central peak position shifts to a higher position. Fig 10 shows the change in central peak position of Cerablak (x=0.75) samples after various anneals.

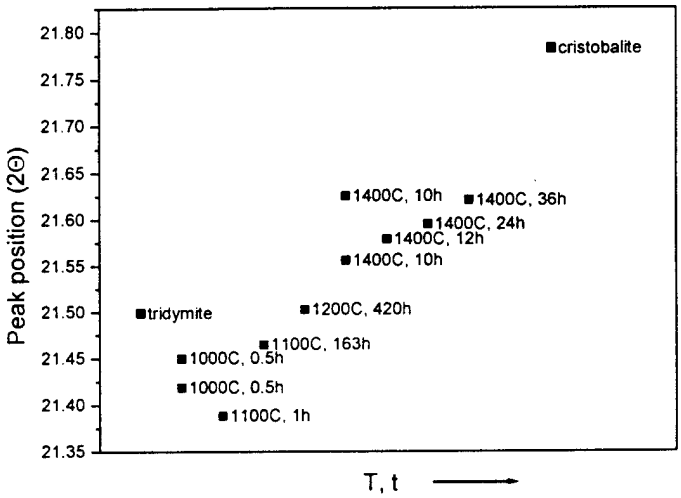

Figure 10. XRD peak shift related to tridymite phase near 21.5° for samples subjected to different annealing schedules.

The crystallite size can also be determined by Scherrer analysis from the x-ray diffraction patterns. As the size of the crystallites become smaller, the half-width of the diffraction peaks becomes broader. The peak near 21.5° can be fit and the full width at half-maximum determined. The size of the crystallite can be calculated. As seen in Table I below, the crystallite size from the Scherrer calculation falls within the same range as the peak width determined from TEM. However, error is introduced because the peak broadening is the result of crystalline disorder as well as crystallite size. For this reason, one author [44] has suggested that the peak at 35° would give more accurate results, but the Cerablak data was too noisy to get reasonable values.

Table I. Nanocrystallite size from TEM images and Sherrer calculations of XRD peaks.

Anneal conditions	**Crystallite size from TEM (nm)**	**Percent crystallinity from TEM**	**Crystallite size from Sherrer calc (nm)**
1100°C, 1h	5-30	25	18
1200°C, 420h	10-50	30-40	67
1300°C, 100h	20-60	30-40	58
1400°C, 10h	20-80	40-50	65

An interesting feature of paracrystalline silicate opals is their resistance to crystallization above 1000°C. This is particularly interesting because the amorphous forms crystallize more readily [36]. This unusual stability of partial disorder is also seen in the aluminum phosphate materials such that their XRD patterns do not change throughout a variety of annealing conditions.

At this point, it is useful to consider the possible role of water in silicate opals and any similarity that may exist between them and the new aluminum rich $AlPO_4$ phases. Opaline water is known to be present in both adsorbed and liquid form as well as silanol groups at dangling oxygens. The molecular water in silicate opals is thought to occur in the disordered regions and it is likely that silanols are more abundant in those regions also [32, 33, 45-46]. Conductivity studies of amorphous $AlPO_4$ thin films have led to the proposal of a dangling oxygen mechanism which is consistent with the presence of bulk -OH groups on either Al or P [47]. If present in Cerablak, these groups are possibly segregated into the amorphous matrix along with excess aluminum around which the hydrogen bearing defects are located. Some authors have found that P=O defects do not exist in $AlPO_4$ [48], implying that hydroxyls occur around a fraction of the aluminum atoms. This idea is substantiated in that ordered domains are found to be 1:1 with respect to the P / Al ratio. Presumably the Al excess becomes concentrated in the amorphous region and contributes to its stability, perhaps by reducing oxygen diffusivity.

Spectroscopic Analysis

In addition to TEM and XRD studies, spectroscopic analysis was carried out to further explore the structure of Cerablak. The bulk of this work was predicated on the presence of P=O being retained to high temperatures. Recent findings (after the end of this project) have shown this to be erroneous, but for the duration of this project, the role of P=O in stabilizing the amorphous structure was studied.

Originally, FTIR done was on Cerablak, both x=0 and x=0.75 (annealed to 1100°C, 1hr), and commercially-available berlinite. Both Cerablak samples showed a strong, sharp peak near 1350 cm^{-1}, while no such peak appeared in the berlinite spectrum. This peak is in the range 1280-1390 cm^{-1} that has been assigned to P=O in a variety of phosphate glasses [49-50]. P=O, as a terminal group, does not appear in crystalline aluminum phosphates. P=O is known to be a constituent in phosphate glasses that disrupt the crystalline network. This

band appears very similar to those in the spectra of binary phosphosilicate glasses, some samples of which are annealed at 800 to 1000 °C [49-50]. Also, various cation-stabilized phosphosilicate glasses are known to have metaphosphate chain structures. These display additional absorbances at around 1000 cm^{-1} and 500 cm^{-1}, corresponding to the presence of P-O-P units [16]. FTIR spectroscopy was done on many other Cerablak powders, as presented in Appendix B. Many powders showed a feature near 1350 cm^{-1}, but not all. This led us to try to determine the relationship between P=O and phase stability.

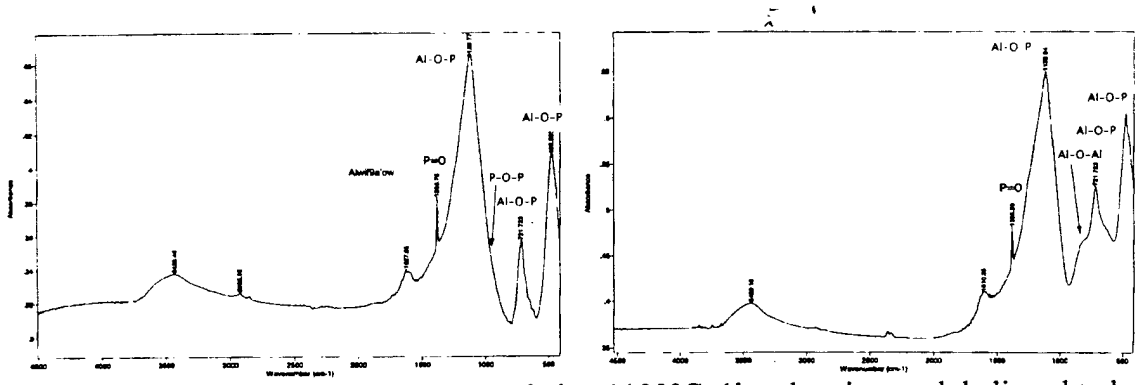

Figure 11. FTIR spectra of Cerablak annealed to 1100°C, 1hr, showing peak believed to be P=O. a) x=0, b) x=0.75

To confirm the presence of P=O, FTIR and Raman spectroscopy was performed by at Arizona State University (ASU) under the guidance of Dr. David Richardson and Prof. George Wolf affiliated with the Department of Chemistry. FTIR studies at ASU did not show the presence of the P=O peaks for annealed powders.

The primary features in the FTIR spectrum are due to Al-O-P (Fig. 12). These are the Al-O-P bending mode at 717 cm^{-1}, the Al-O-P stretch at 1120 cm^{-1} and its rocking mode at 472 cm^{-1}. In addition to these features, some features showing Al-O-Al and P-O-P linkages were present at ~800 cm^{-1} and ~1000 cm^{-1}, respectively. Cerablak (x=0) annealed 1100°C, 1h shows a strong presence of P-O-P and a weak feature for Al-O-Al [51, 52]. P-O-P is also seen in C-1.25 1100°C, 1hr, and extremely weak feature in C-1.5 suggesting P-O-P content decreases with increasing aluminum content. Correspondingly, the amount of Al-O-Al increases with increasing Al content (Table II). These results suggest that phase segregation of P-rich and Al-rich species does occur at the precursor stage. It is suspected that the driving force for these associations is related to the formation of energetically favorable Al-rich Al-O-P complexes. The presence of very small amounts of Al-O-Al even in the stoichiometric C-1 sample supports the hypothesis of phase segregation in the precursor.

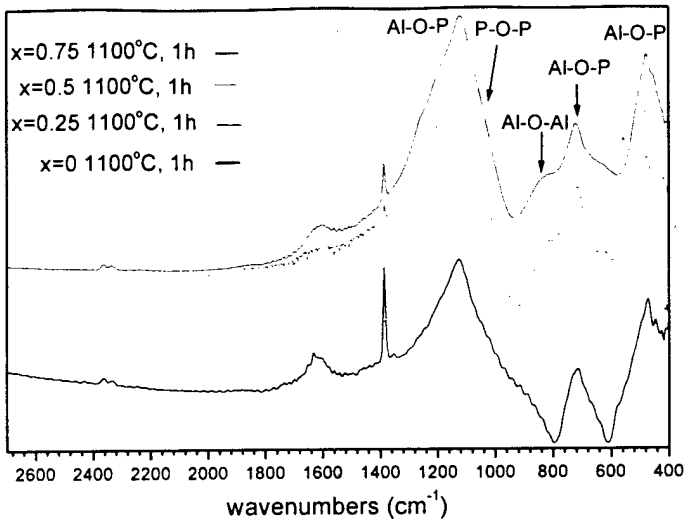

Figure 12. FTIR spectra of Cerablak powders, showing presence of P-O-P and Al-O-Al with aluminum content.

Table II. Relative amounts of Al-O-Al in Cerablak powders with aluminum content and anneal temperature.

Composition	**Anneal Schedule**	**Area ratio of peak near 800 to peak near 715 cm^{-1}**
C-1	1100°C, 1h	0.0529
C-1.25	1100°C, 1h	0.3778
C-1.5	1100°C, 1h	0.5781
C-1.75	1000°C, 0,5h	0.1188
C-1.75	1100°C, 1h	0.7836

FTIR of both x=0 and x=0.75 powders also indicate the presence of two types of OH groups; one at 3400 cm^{-1} assigned to bulk silanol analogs and another at 3200 cm^{-1} resulting from molecular water [53, 54]. Another band at around 1600 cm^{-1} confirms the presence of water. Proof that the other -OH is an actual "Alanol" (Al-OH) group depends upon identification of another absorption at 4500 cm^{-1}, which results from a combination of stretching and bending modes [53]. This Al-O-H bend should appear at 950 cm^{-1} but is not seen even in the C-1.75 sample, suggesting that the OH bands relate to presence of water presumably trapped in the amorphous network. It is suspected that the source of water is from the water of hydration present in the aluminum nitrate added to the precursor.

Raman spectroscopy was used to confirm the presence of P=O. Berlinite was used as a standard to determine peaks associated with crystalline aluminum phosphate. Most Cerablak samples did not show these crystalline peaks. Most Cerablak Raman spectra showed two prominent peaks at 1350 and 1600 cm^{-1}.. The Raman used was a micro Raman, with the ability to focus on a small area (~5μm) of the sample.

The overall color of the powder samples can be described as black or varying shades of gray. However, when looking closely at the gray powders, it is apparent that the sample is a mixture of white and black particles. With the microRaman laser, Prof. Wolf (ASU) was able to collect spectra from the overall sample, and from predominately white and predominately black areas. These spectra showed the presence of the two peaks in the black areas and weak crystalline peaks in the white particles even for the same sample.

One unusual feature of the Raman spectra was the presence of a peak at 1350 cm^{-1} (attributed to P=O) and a peak at 1600 cm^{-1} (attributed to –OH). When molecular water is present in the sample, there is an accompanying peak near 3500 cm^{-1}. However, in Cerablak, the peak at 3500 cm^{-1} was not present, and the peaks at 1350 and 1600 cm^{-1} scaled with each other. Dr. Wolf suggested the possibility of a resonance Raman effect with the P=O and water that was increasing the intensity of the peak at 1600 cm^{-1}. Since the end of this project, it has been determined that the Raman features at 1350 and 1600 cm^{-1} are from elemental carbon, not P=O and water. It has also been determined that the sharp peaks near 1390 cm^{-1} in some FTIR spectra were from atmospheric contamination, and do not indicate the presence of P=O.

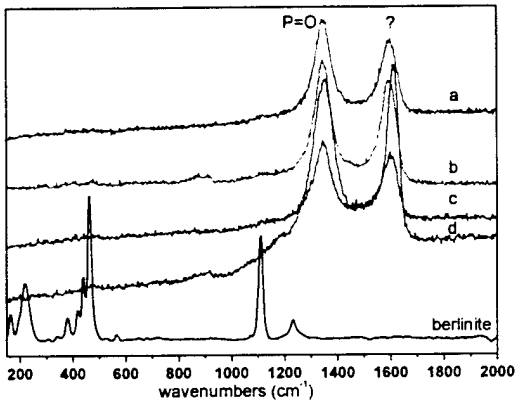

Figure 13. Raman spectra of Cerablak powder (x=0.75) annealed to various temperatures a 1400°C, 10h b 1300°C, 100h c 1200°C, 100h d 1100°C, 1h; all show strong P=O absorbance compared to crystalline berlinite. Measurements taken with a 514.531 nm laser at 0.35 mW, HV depolarized.

FTIR and Raman were also done on C-1.75 gel dried at 150°C, and annealed to 250°C, 500°C, 750°C and 1000°C (Fig. 14, 15). The FTIR shows that P=O is present after drying at 150°C, but disappears after 250°C anneal. There also appears to be some P-O-P content in the dried gel, which also disappears after anneal at 250°C.

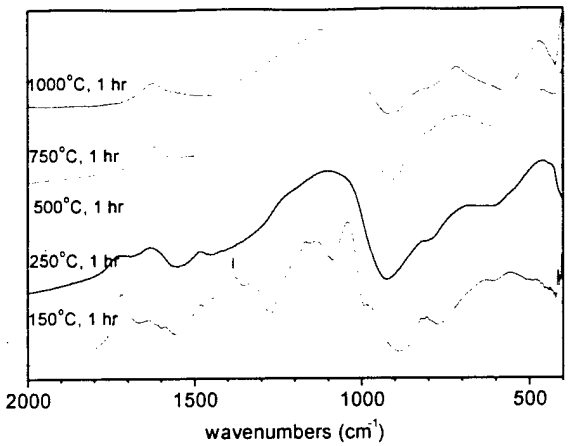

Figure 14. FTIR of dried gel and after anneal at low temperatures.

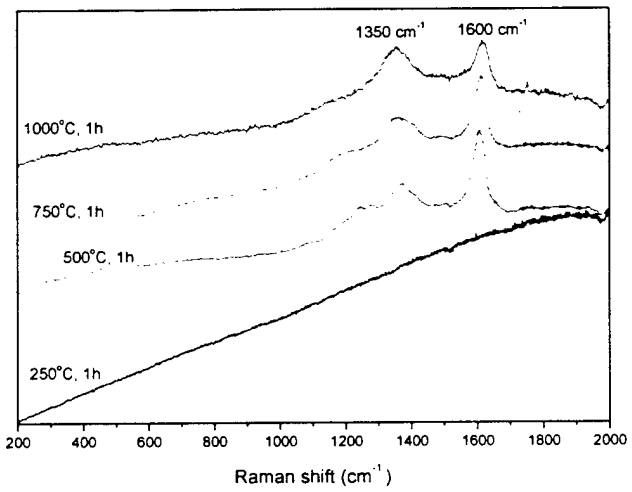

Figure 15. Raman of dried gel, showing carbon formation beginning at 500°C.

Precursor Stability and Characteristics

Based on the collective evidence presented above, it is evident that molecular events occurring at the precursor stage plays a significant role in controlling the phase content upon pyrolysis. Two issues were studied related to the precursor formulation as discussed below:

Solution Aging

Another interesting development is the effect of solution age on the amorphous content of Cerablak powder. Solutions that have been refrigerated for many months, or solutions that have been aged at room temperature show a greater degree of amorphous character than freshly-made solutions when annealed at 1000°C for ½ hour. Figure 16 shows typical XRD patterns of aged and freshly synthesized Cerablak powder. The aged solution (refrigerated for 21 months prior to anneal), upon pyrolysis, yields powder that show typical amorphous XRD pattern with a broad feature near 20 degrees, whereas powder made from freshly synthesized solution shows a typical Cerablak XRD pattern that account for the presence of

the nanocrystallites and amorphous matrix. The effect of solution aging on amorphous content is less obvious with higher temperature anneals. After 1100°C, 1hr anneal the 21-month-old solution shows the XRD pattern to be similar to Cerablak, but less defined than a fresh solution. It is not yet clear what the role of aging is on the decomposition behavior. Concentration appears to have an effect on aging as well. A solution with higher concentration appear to age faster than dilute solutions. Precursor characterization of the aged solutions are underway to determine the nature of the species present and any associated differences with freshly-prepared precursor solutions.

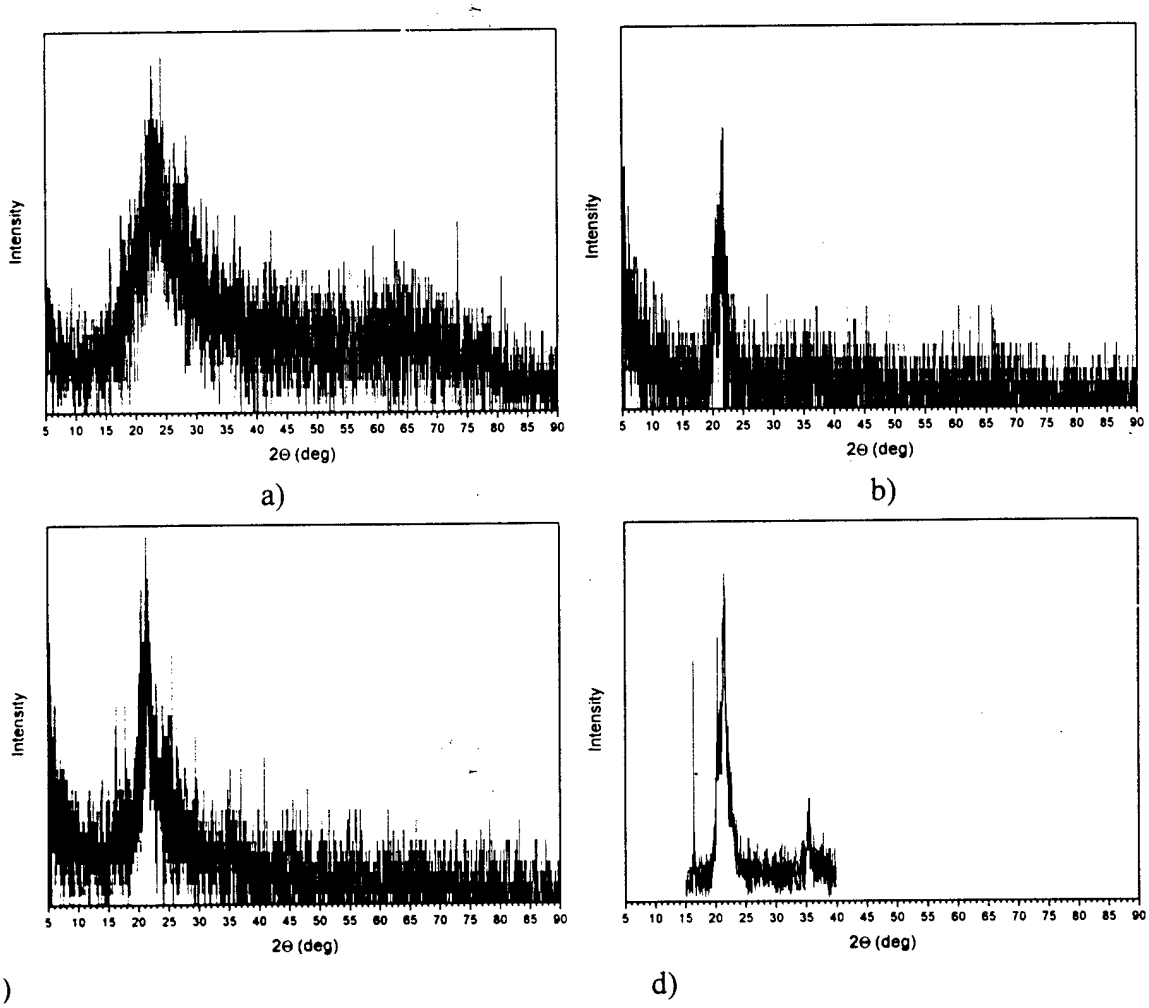

Figure 16. XRD patterns of refrigerated-aged solutions a) 21 months; 1000°C, 0.5h b)21 months; 1100°C, 1h. c) 15 months; 1000°C, 0.5 h d) 15 months; 1100°C, 1h (Note that the sharp feature near 16° is an artifact)

Synthesis under ambient conditions

Normally, Cerablak is synthesized inside a dry glove box. The P_2O_5 is highly hygroscopic and will absorb atmospheric moisture readily. However, the requirement of a dry atmosphere would adversely impact scale-up and processing of large quantities. Previous

experiments have shown that it may not be necessary to synthesize Cerablak precursor under very dry conditions. To test the sensitivity of the synthetic process, Cerablak precursor was formulated in ambient air. Three experiments were performed: a) dissolving P_2O_5 slowly in ethanol and then mixing with aluminum nitrate solution, b) letting P_2O_5 exposed to the ambient until it became a "soupy" liquid and then dissolving in ethanol, and c)adding the P_2O_5 directly to the aluminum nitrate solution. All of these variants resulted in Cerablak, after 1100°C, 1 hr anneal.

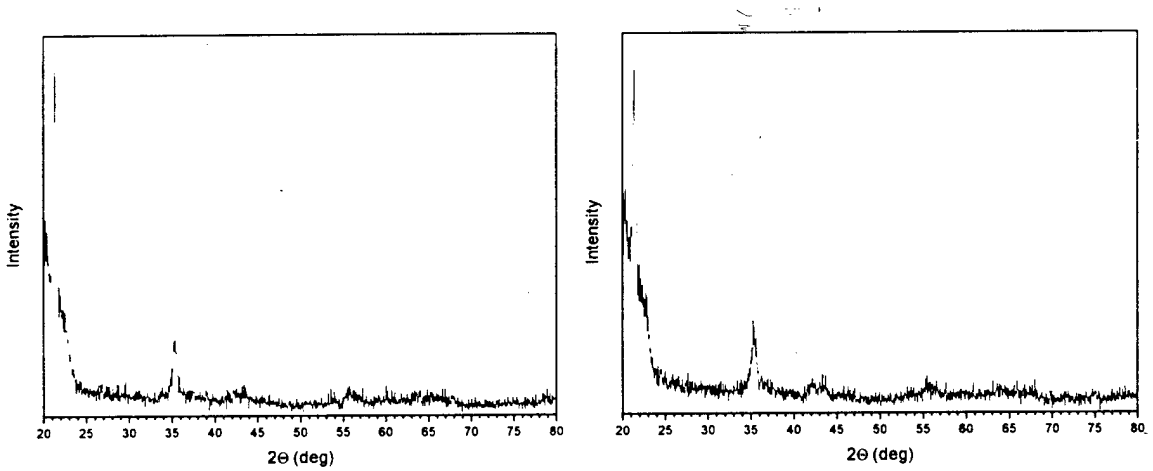

Figure 17. XRD patterns of Cerablak (x=0.75) after 1100°C, 1hr anneal. a) P_2O_5 in ethanol prepared in ambient air and added to aluminum nitrate solution and b) P_2O_5 added directly to aluminum nitrate ethanolic solution.

Synthetic Forms and Uses

In order to utilize the unique properties and behavior of Cerablak for various applications, some efforts were employed to explore the various synthetic forms of Cerablak. In addition, bulk materials are desired to measure certain properties. Attempts were successful in synthesizing Cerablak in various forms including powder, thin and thick films, bulk consolidated material, and fibers. Cerablak powder is formed directly from annealing dried solution. The powder can be used for characterization studies, plasma sprayed to develop thick coatings on metal or alloy substrates, or electroconsolidated into near-net shaped dense bodies (~20 % porosity).

Near Net-shaped Cerablak Bodies

Earlier attempts to synthesize dense Cerablak materials were not successful since Cerablak powder does not sinter at high temperature presumably due to low atom mobility. However, a new electroconsolidation process developed by Superior Graphite Inc., appear to be suitable to prepare dense Cerablak bodies. In this process, the powder was subjected to 1350°C for 30 minutes while under ultra-high isostatic pressure with high purity graphite powder as the pressure medium. In principle, there is no difference between the electroconsolidation and hot pressing processes except that the electroconsolidation was

especially developed to fabricate near-net shape articles. It is not clear why the hot pressing experiments did not yield dense bodies. However, this study shows that near-net shape Cerablak solid components can be fabricated for specific applications.

Cerablak Matrix material for Ceramic Matrix Composites (CMCs)

In collaboration with Mcdermott Technology, Inc., ATFI is investigating the use of Cerablak as a stable high temperature matrix material for use in CMCs. Fiber strength degradation during matrix processing is a significant concern for the CMC community. In addition, low cost fabrication methods to obtain dense oxide matrices is critical to implementation of CMCs in many military and commercial applications. Cerablak offers many advantages including a) suitable precursor with high yield and low viscosity for efficient infiltration, b) stable and compatible chemistry that limit fiber strength degradation, c) low density (2-2.2 g/cm^3) to make lightweight CMCs for aerospace applications, d) low dielectric constant for low observable applications (see below), and e) compatibility with most oxide CMC constituents

Rich Goettler of McDermott Technology Inc. (MTI) has fabricated CMC test panels using unidirectional fiber lay-ups with alumina and Cerablak matrices. A Cerablak/alumina slurry was infiltrated into a fabric with no interface coating. The composite showed excellent strength retention after annealing at 1100°C, 1h. The tensile strengths ranged from 60-90 ksi with linear stress-strain behavior. Densities of these composites had open porosity ranging from 8-15 %. These results are very encouraging and has prompted AFRL to pursue Cerablak matrices for monazite-coated CMCs. Further results are pending on new composite panels fabricated by MTI.

Plasma-Sprayed Cerablak Coatings

For some applications, thick Cerablak coatings may be desired and plasma spray process has been extensively used in the coatings industry. It is a versatile process and offers very high deposition rates. A few experiments were done to determine the feasibility of plasma spray coatings. Cerablak powder was used to develop plasma spray coatings on steel and cast iron. Preliminary analysis of the coating show the coating to be fairly adherent with good coverage and the phase analysis by XRD show the coatings to primarily contain Cerablak which is quite remarkable considering partial melting that occur when the powder is subjected to high temperature plasma. Surface morphology of the plasma spray deposits does indicate the material was partially melted during the coating process.

Cerablak Fibers

Cerablak fibers may have high high-temperature strength and creep resistance desired for reinforcements used in high temperature ceramic matrix composites. In general, amorphous fibers are very strong (low flaw population) but suffer from poor creep resistance even at moderately high temperatures due to viscous flow. Other amorphous fibers studied in the past also suffer from devitrification at moderately low temperatures (below 1000°C) such that they are not useful as high temperature reinforcements. The ability of Cerablak to remain amorphous to very high temperatures combined with low atom mobility raises the possibility for its use as strong and creep resistant fiber reinforcements in composites. Preliminary work

to synthesize Cerablak fibers from a polymeric precursor was fairly successful. Cerablak fiber precursor derived by concentrating the solution is a viscous, clear liquid from which fibers can be pulled by simply inserting and retracting a needle. The precursor is made by concentrating Cerablak solutions in a rotary evaporator to approximately 30 wt%. Adjusting the precursor concentration prior to the decomposition for making fibers is very important. If the concentration is not high enough, the resulting precursor may not be viscous enough to pull fibers. If the solution becomes too concentrated, the resulting precursor becomes too stiff to pull fibers.

Fiber precursor also seems to be affected by atmospheric humidity. If it is too humid, the precursor seems to absorb water and the viscosity decreases. If the precursor is kept in a dry box, it becomes too stiff to pull fibers. It is important to thoroughly cover the precursors with parafilm, or an equally waterproof cover. It has also been noticed that a change in atmospheric humidity can restore a fiber precursor to the correct viscosity. Fibers pulled from appropriately-tailored precursor characteristics are smooth and dense. They range in diameter from 1-50 μm. Very long fibers (3+ ft.) can be pulled, but the ventilation in the laboratory prevents us from collecting long fibers. Cross-sectional SEM images show that the fibers are dense and smooth when pulled from a clear precursor (Fig 18). However, fibers become porous when pulled from a precursor which is "foamy".

a) b)

Figure 18. SEM micrographs of Cerablak fibers a) pulled from clear precursor b) pulled from foamy precursor.

Annealing studies were also conducted on the fibers to assess their integrity and thermal stability. The fibers were originally annealed at 900°C. Some fibers were further annealed at 1100°C, 1hr, 1200°C, 10 hr and 1200°C, 100 hr. After anneal up to 1200°C, 10hr, the fibers remained black, smooth and dense. EDS analysis showed P/Al ratios the same as fibers annealed at 900°C. However, after anneal at 1200°C, 100h, some of the fibers turned white. Most of the fibers contained both black and white areas within the same fiber. EDS analysis of the surface showed substantial phosphorus loss. Some fibers retained some phosphorus, while others retained none (Fig. 19). The thermal behavior of the pulled fibers appears to be

different from the powder materials. The powders, even after 36h at 1400°C did not show any P loss from the surface. It is not clear if this is related to varying surface chemistry during precursor pyrolysis in the two cases.

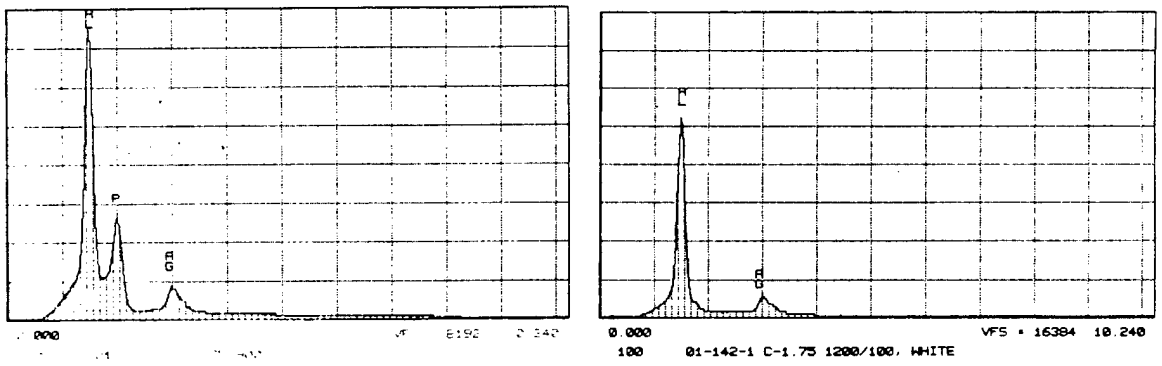

a) b)

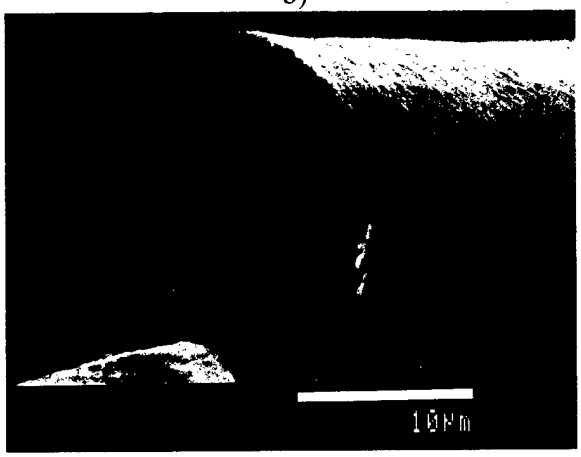

c)

Figure 19. a) EDS of fiber surface after 900°C, 1h anneal. b) EDS of fiber surface after 1200°C, 100h anneal, showing loss of phosphorus. c) SEM micrograph of fiber after 1200°C, 100h anneal.

As there is a need for better optical fiber amplifiers which typically consist of < 1 wt % erbium in amorphous host materials, few attempts were made to synthesize erbium-doped Cerablak fibers. However, the presence of erbium nitrate in the precursor destabilized the chemistry upon heating resulting in precipitated or colloidal fiber precursor which did not yield good quality fibers.

Cerablak Protective Coatings

Perhaps the best potential for Cerablak's use in industry will be to exploit its protective ability under oxidation, corrosion, and harsh environmental conditions. Metals, alloys and ceramics are being used in a wide variety of environments and are susceptible to degradation. The Cerablak precursor is very suitable to deposit smooth, dense, and adherent coatings on a variety of substrates. Cerablak's inert nature and low oxygen permeability can be useful in

providing adequate protection. Coatings can be produced using a simple dip-coating process with subsequent annealing. Many different stainless steel samples were dip coated with Cerablak. Concentration and solution age were varied. Coated pieces were annealed at 1000°C in air for 10-100 hours to test oxidation protection. Many coatings did not confer significant protection primarily due to cracking resulting from drying and/or thermal stresses generated during cooling. A thick coating (> 1 μm) would invariably crack uniformly while thinner coatings were almost crack-free except in few locations. Optical microscopy was used primarily to analyze the distribution of the coating on all substrates

Cerablak-coated and uncoated 304 stainless steel coupons were exposed to oxidation at elevated temperatures to test Cerablak's protective ability. The coated coupons showed a dramatically lower weight gain (0.08% - 0.24%, including the weight of the coating) than the uncoated coupons (4.6% - 8.64%). One set of samples was subjected to 3 additional cycles of heating to 1000°C for 1 hour and a final cycle of 1000°C for 10 hours to test ability to withstand thermal cycling. Even after repeated cycling, the coated coupon showed little weight gain compared to the uncoated piece (Table III). Figure 20 shows photographs of one set of coupons, at the end of repeated thermal cycles.

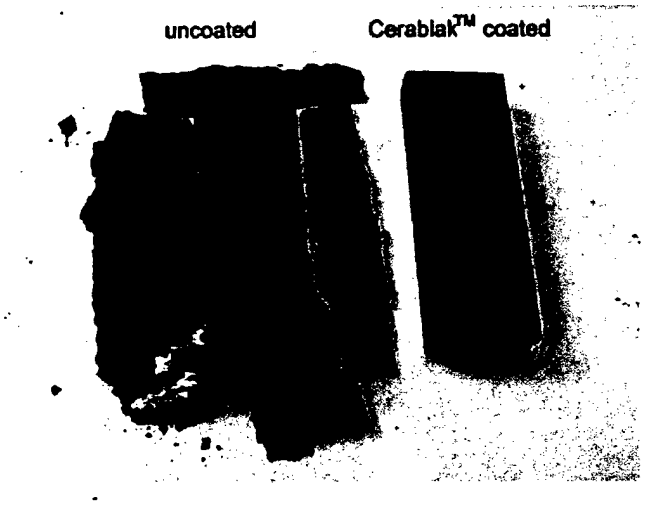

Figure 20. Uncoated and Cerablak coated stainless steel coupons after anneal at 1000°C for 100 h.

Table III. Weight gain of uncoated, and Cerablak coated stainless steel coupons annealed to 1000°C in air. The anneals were progressive, using the same samples. The weight gain is related to the weight of the unannealed, uncoated coupon.

Sample	**Anneal Schedule (progressive)**				
	100 hr	1 hr	1 hr	1 hr	10 hr
Cerablak coated (including coating)	0.24%	0.27%	0.30%	0.33%	0.45%
Uncoated	8.64%	8.69%	8.80%	8.82%	9.06%
Cerablak	0.088%				
Uncoated	4.60%				

In addition to stainless steel, Cerablak was also tested as a protective coating on other metals. Nickel aluminide superalloy coupons with MCrAlY bondcoat were coated with Cerablak for an industrial client. Thermal cycling tests of 1100°C for 1 day were performed. Typically, the bondcoat develops a 10 micron-thick alumina scale in each cycle, which spalls off upon cooling. A Cerablak-coated coupon lasted for 18 days (18 cycles) before the oxide scale grew thick enough to spall off.

Cerablak Interface Coatings for CMCs

Minicomposites with Cerablak interface coatings on Nextel 610 fibers were fabricated and tested by AFRL (Tap Parthasarathy, Dayton, OH). Minicomposites annealed to 1100°C for one hour show good strength retention and promising interface properties (debonding behavior) (Fig. 21).

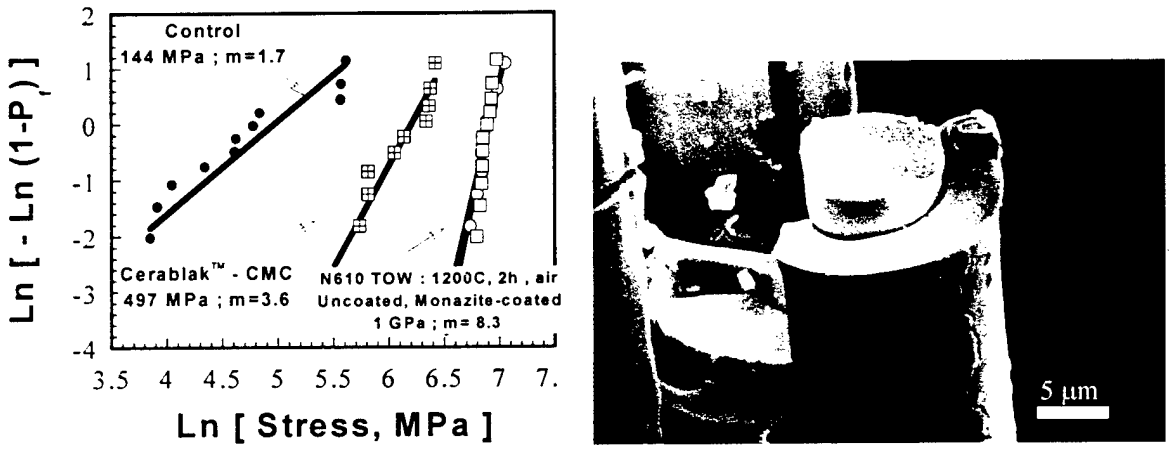

a) b)

Figure 21. Ceramic matrix minicomposites with Cerablak interface layer and alumina matrix. a) Weibull plot showing tensile strength of composites with Cerablak, monazite and no interface coating. b) Fracture surface of Cerablak coated composite.

Cerablak Properties

Thermal Expansion

Thermal expansion of an electroconsolidated Cerablak pellet was measured by dilatometry from room temperature to 1100°C (Fig 22). The thermal expansion coefficient of Cerablak is considerably low, around 5 $x10^{-6}$ /K. This can present problems with coating metal (CTE type 304 stainless steel = $17x10^{-6}$ /K), because of the large thermal stresses upon annealing and cool down.

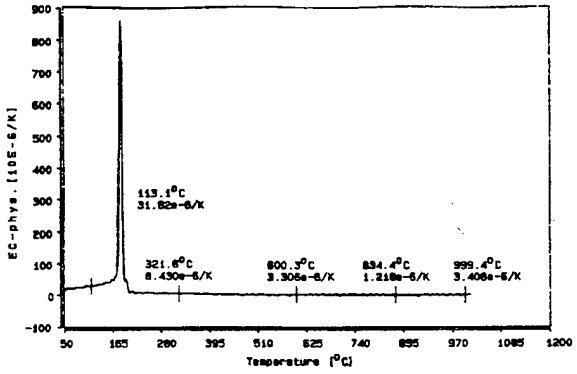

Figure 22. Thermal expansion of an electroconsolidated Cerablak pellet.

Thermal conductivity of Cerablak

Holometrix, Inc measured thermal conductivity from room temperature to 1300°C on a 0.5 in x 1mm sample of a consolidated Cerablak material (not fully dense). The thermal conductivity is low (1-1.5 W/mK). Figure 23 shows the comparison with many refractory oxides, including dense YSZ, a commonly used thermal barrier coating material. Low thermal conductivity is due to the amorphous content of the material, and the consequent disruption of phonon conductivity. The low thermal conductivity suggests that Cerablak may be a viable thermal barrier coating as well as an oxidation barrier.

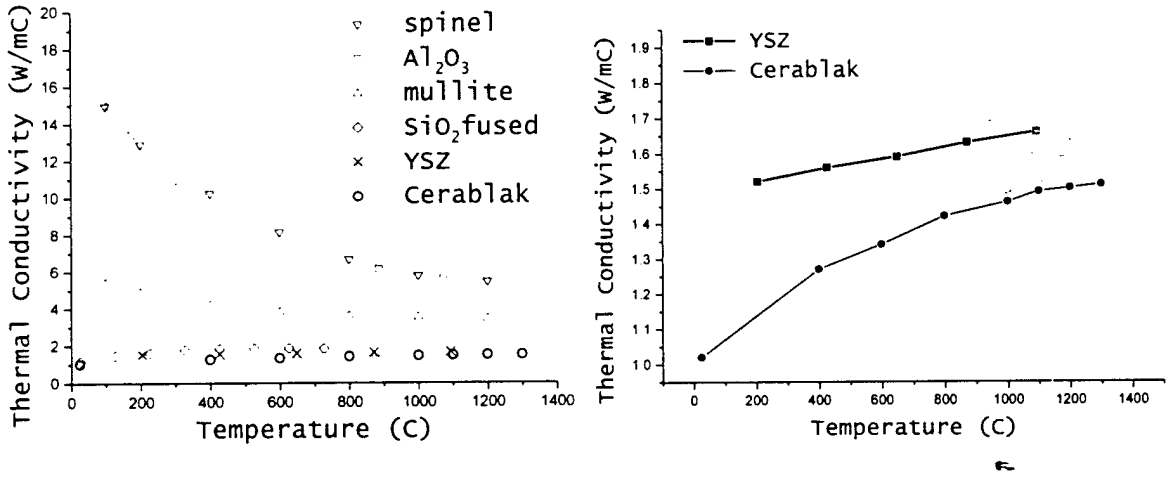

a) b)

Figure 23. a) Thermal conductivity of Cerablak (lower line) with YSZ, fused silica, mullite alumina and spinel. b) Thermal conductivity of Cerablak (lower line) and YSZ, a common thermal barrier material.

Dielectric Constant

Based on our estimated low dielectric constant value for Cerablak, Dr. Larry Matson of AFRL, Dayton, OH expressed an interest in examining this material for window and other

classified applications. Powders of various compositions and a piece of consolidated material were supplied to AFRL for testing over a range of high frequencies. While all compositions exhibited low values, C-1.5 was the lowest at 3.3 which looks very promising (Table IV). As these powders contain at least 20-30% of crystalline inclusions, it will be interesting to explore the dielectric properties of pure amorphous films of Cerablak.

Table IV. Dielectric constant of Cerablak

Cerablak composition	**Average**
C-0.75	4.35
C-1.1	5.91
C-1.25	4.95
C-1.5	3.34
C-1.75 electroconsolidated	5.7
C-10	5.33

Compatibility with silica and SiC

Compatibility of Cerablak with SiC and silica was determined for possible applications as a protective coating for silicon carbide composites. Compatibility tests conducted previously with coated SiC powders indicated the two materials to be compatible to at least 1100°C. However, recent experiments done using coated SiC fibers and coated silicon wafers show the material to react with silica above 1200°C. Cerablak coated SiC tows (CG Nicalon, Tyranno ZMI, and Tyranno SA) have been annealed to 1200°C for 100 hours. SEM investigation has shown that Cerablak may be incompatible with SiC at high temperatures for extended periods of time (Fig 24a).

Cross-sectional TEM analysis performed on silicon-coated wafers shows Cerablak decomposing to an alumina phase with most of the phosphorus lost (Fig. 24b).

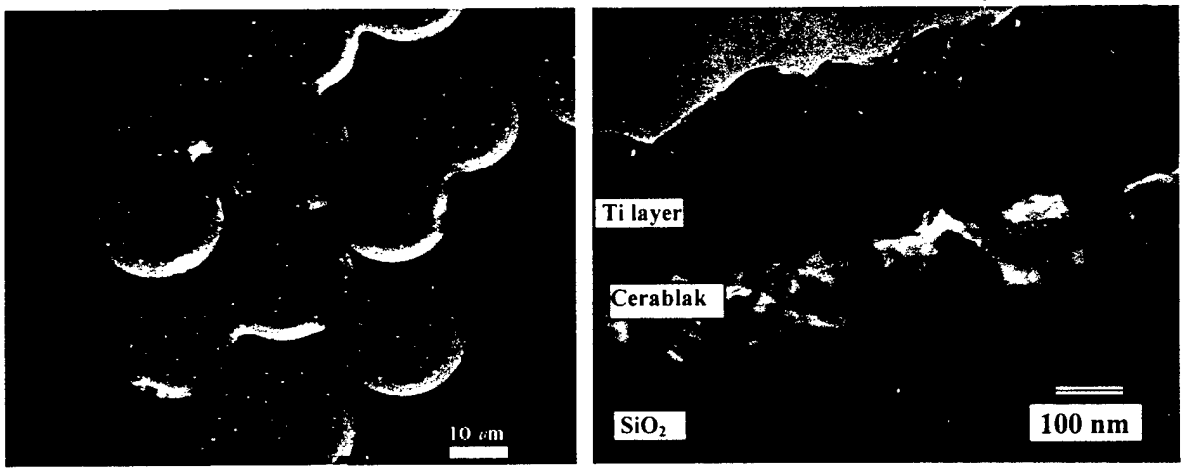

a) b)

Figure 24. a) Cerablak coated SiC fiber. The Cerablak has reacted with the silica during anneal to 1200°C for 100 hr. b) TEM micrograph of Cerablak coated silicon annealed to 1200°C for 180 hr, where the Cerablak has decomposed. The titanium was deposited to aid sample preparation.

Other Applications

Nanocrystalline Cerablak Matrix Composites (NCMCs)

Analysis of various Cerablak powders has shown presence of nanocrystalline inclusions (alumina, calcium tungstate, erbium phosphate, and aluminum phosphate) in an amorphous Cerablak matrix. We believe synthesis of these NCMCs has significance for many applications. The inclusions can provide hardness, toughness, lubricity, etc. and, in addition, they may be useful in tailoring CTE such that Cerablak protective coatings can be used with a wide range of metal/alloy substrates.

Erbium doped Cerablak

Many research groups have tried to develop 1-3% erbium-doped amorphous aluminum phosphate with little success [55-57]. Erbium-doped materials are in demand for optical amplifiers for photonic amplifications. An amorphous material is desired for the host because there is less interference with the photons than with a crystalline material. We have shown by x-ray diffraction that 5% erbium-doped (relative to aluminum content) does not precipitate erbium-containing species when annealed to 1000°C for ½ hour (Fig 25). This result opens the opportunity of developing erbium-doped amorphous Cerablak fibers, which will be useful for fiber lasers. After anneal at 1100°C for 1 hour, nanocrystallites of $ErPO_4$ were formed.

Recent work in France suggests that nanocrystalline inclusions in amorphous matrix may provide much better gain properties than dissolved erbium for fiber and waveguide amplifiers [58]. Both approaches may be suitable with Cerablak. TEM results of the 5mol% Er-doped Cerablak annealed to 1000°C for 1 hour shows a large nanocrystal fraction (Fig. 26). The nanocrystalline fraction is greatly increased over pure Cerablak.

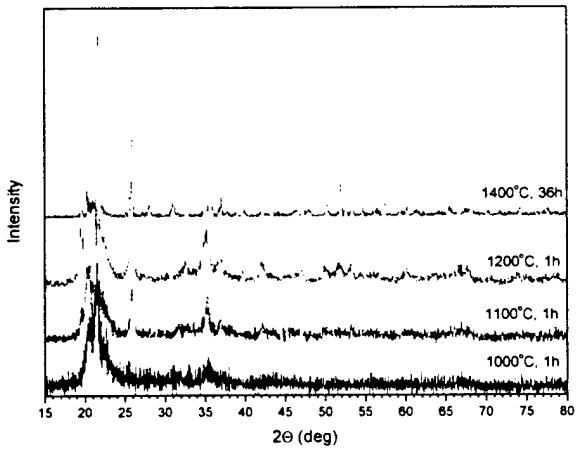

Figure 25. XRD pattern of 5mol% Er-doped Cerablak after anneal under various conditions, showing the crystallization of $ErPO_4$.

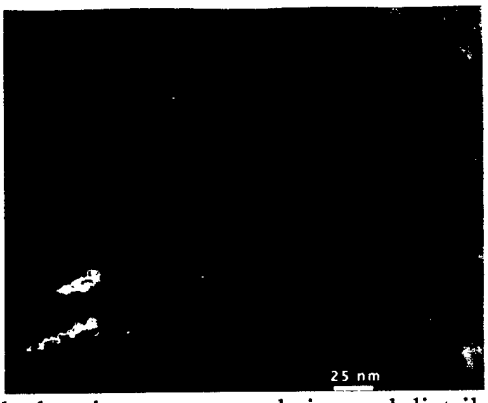

Figure 26. TEM micrograph showing nanocrystal size and distribution in 5mol% Er-doped Cerablak annealed 1000°C, 1h.

Non-stick coating for molten aluminum processing

Cerablak™ has been shown by two industrial clients to be non-wetting to molten aluminum. A cast iron tube was dip-coated with Cerablak™ and immersed, along with a standard enamel-coated cast iron tube in an industrial molten aluminum bath. The tube was initially removed for visual inspection after 2 days in the bath. Upon being raised from the bath, the aluminum slid off the Cerablak coated tube. This non-stick behavior was remarkable, since molten aluminum sticks very well to the enamel surface or other metal/glass-based TPTs. Both tubes were re-immersed in the bath for an additional 3 days. After a total of 5 days in the bath, both tubes were removed and cross-sectioned. The enamel-coated tube showed extensive degradation and pitting, as was expected. The Cerablak-coated tube showed no degradation or pitting

References

1. J. Eckert, G. D. Stucky, and A. K. Cheetham. *Mat. Res. Bull.*, **24** (5) 31 (1999)
2. Chen, Yu-Wen, Wen-Cheng Hsu and Chiang-Shiang Lin, "Hydrodesulfurization Reactions of Residual Oils over CoMo/Alumina-Aluminum Phosphate Catalysis in a Trickle Bed Reactor," *Ind. Eng. Chem. Res.*, **29**, 1830-1840, 1990.
3. Cheung, T. T. P., K. W. Willcox, M. P. McDaniel, M. M. Johnson, C. Bronnimann and J. Frye, "The Structure of Coprecipitated Aluminophosphate Catalyst Supports," *J. Catal.*, **102**, 10-20, 1986.
4. Balkus, Jr. Kenneth J., Laura J. Sottile, Scott J. Riley, Bruce E. Gnade, "The preparation and characterization of $AlPO_4$ thin films via laser ablation of $AlPO_4$-H_4," *Thin Solid Films*, **260**, 4-9, 1995.
5. A. Bandyopadhyay, and P. B. Aswath, *J. Mat. Sci.*, **29**, 4205 (1994)
6. M. Fishkis, J. R. Yeh, and K. Wefers *J. Mat. Sci.*, **29** 110 (1994)
7. Li, Chiuping, Yu-Wen Chen and Ming-Chang Tsai, "Highly Restrictive Diffusion under Hydrotreating Reactions of Heavy Residue Oils," *Ind. Eng. Chem. Res.*, **34**, 898-905, 1995.
8. Marcelin, George, Roger F. Vogel and Harold E. Swift, "Alumina-Aluminum Phosphate as a Large-Pore Support and Its Application to Liquid Phase Hydrogenation," *J. Catal.*, **83**, 42-49, 1983.
9. Menon, R., H. S. Joo, J. A. Guin, P. J. Reucroft and J. Y. Kim, "Evaluation of Alumina-Aluminum Phosphate Catalyst Supports for Hydrodenitrogenation of Pyridine and Coal-Derived Liquids," *Energy & Fuels*, **10**, 579-586, 1996.
10. Smith, K. J., Leszek Lewkowicz, Mike C. Oballa and Andrzej Krzywicki, "Effect of Pore Size on Bitumen Hydrocracking Over Al_2O_3- $AlPO_4$ Supported Ni-Mo Catalysts," *Can. J. Chem. Eng.*, **72**, 637-643, 1994.
11. Tsai, Ming-Chang and Yu-Wen Chen, "Restrictive Diffusion under HydrotreatingReactions of Heavy Residue Oils in a Trickle Bed Reactor," *Ind. Eng. Chem. Res.*, **32**, 1603-1609, 1993.
12. He, Q., S. Lafrenière, S. I. Najafi and S. Honkanen, "Rare Earth (Nd^{3+}, Er^{3+} and Yb^{3+}) Doped Aluminum Phosphate Sol-Gel Films," *SPIE*, **1794** Integrated Optical Circuits II, 303-308, 1992.
13. Goiffon, Aline, Jean-Claude Jumas, Maurice Maurin and Etienn Philippot, "Etude comparée à diverses températures (173, 293 et 373°K) des structures de type quartz α des phases $M^{III}X^{V}O_4$ (M^{III} = Al, Ga and X^{V} = P, As)," *J. Solid State Chem.*, **61**, 384-396, 1986.
14. Kosten, Klaus and Heinrich Arnold, "Die III-V-Analoga des SiO_2," *Zeitschrift Kristallographic*, **152**, 119-133, 1980.
15. Magneron, N., Y. Luspin, G. Hauret, and E. Philippot, "Investigation of $AlPO_4$ by Brillouin Spectroscopy from 300 to 1100 K," *J. Phys. I France*, **7**, 569-580, 1997.
16. Muraoka, Y. and K. Kihara, "The temperature dependence of the crystal structure of berlinite, a quartz-type form of $AlPO_4$," *Phys Chem Minerals*, **24**, 243-253, 1997.
17. Ng, H. N. and C. Calvo, "X-ray study of the α-β transformation of berlinite ($AlPO_4$)," *Can. J. Phys.*, **54**, 638-647, 1976.
18. Ng, H. N. and C. Calvo, "X-ray study of the twinning and phase transformations of phosphocristobalite ($AlPO_4$)," *Can. J. Phys.*, **55**, 677-683, 1977.

19. Philippot, E., A. Goiffon, A. Ibanez and M. Pintard, " Structure Deformations and Existence of the α-β Transition in MXO_4 Quartz-like Materials," *J. Solid State Chem.*, **110**, 356-362, 1994.
20. Philippot, E., D. Palmier, M. Pintard and A. Goiffon, "A General Survey of Quartz-like Materials: Packing Distortions, Temperature, and Pressure Effects," *J. Solid State Chem.*, **123**, 1-13, 1996.
21. Phillips, Brian L., John G. Thompson, Yuehui Xiao and R. James Kirkpatrick, "Constraints on the Structure and Dynamics of the β-Cristobalite Polymorphs of SiO_2 and $AlPO_4$ from ^{31}P, ^{27}Al, and ^{29}Si NMR Spectroscopy to 770K," *Phys Chem Minerals*, **20**, 341-352, 1993.
22. Tendeloo, G. van, J. van Landuyt and S. Amelinckx, "The α-β Phase Transition in Quartz and $AlPO_4$ as Studied by Electron Microscopy and Diffraction," *Phys. Stat. Sol. (A)*, **33**, 723-735, 1976.
23. Thong, Ngo and D. Schwarzenbach, "The Use of Electric Field Gradient Calculations in Charge Density Refinements. II. Charge Density Refinement of the Low-Quartz Structure of Aluminum Phosphate," *Acta Cryst.*, A**35**, 658-664, 1979.
24. Prabakar, S., K. J. Rao and C. N. R. Rao, "A Study of $AlPO_4$ By ^{27}Al and ^{31}P MAS NMR Spectroscopy," *Mat. Res. Bull.*, **26**, 805-812, 1991.
25. Watson, G. W. and S. C. Parker, "Dynamical instabilities in α-quartz and α-berlinite: A mechanism for amorphization," *Phys. Rev. B*, **52** (18), 13 306 - 13 309, 1995.
26. M. A. Harmer and A. J. Vega, *Solid State Nuclear Magnetic Resonance*, **5**, 35 (1995).
27. Sanz, J., J. M. Campelo and J. M. Marinas, "NMR Characterization of Synthetic and Modified Aluminum Orthophosphates," *J. Catal.*, **130**, 642-65, 1991
28. P. E. Stone, E. P. Egan, Jr., and J. R. Lehr, *J. Am. Ceram. Soc.* **39**[3] 89 (1956).
29. I. V. Tananaev, E. V. Maksimchuk, Yu. G. Bushuev, and S. A. Shestov, *Inorg. Mater.*, **14**[4] 562 (1978).
30. M. Harmer, A. J. Vega and R. B. Flippen. *Chem. Matl*, 6 (11) 1903 (1994).
31. Blackwell, C. S. and R. L. Patton, "Aluminum-27 and Phosphorus-31 Nuclear Magnetic Resonance Studies of Aluminophosphate Molecular Sieves," *J. Phys. Chem*, **88**, 6135-6139, 1984.
32. D. K. Smith, Powder Diffr., 13(1), 2-19, (1998).
33. H. Graetsch, Reviews in Mineralogy, Mineralogical Society of America, Washington, D.C., 29, 209-232, (1994).
34. G. Guthrie, D. L. Bish, R. C. Reynolds, American Mineralogist, 80, 869-872, (1995).
35. K. Kano, Geochemical Journal, 17, 87-93, (1983).
36. H. Graetsch, H. Gies, and I. Topalovic, Phys. Chem. Minerals, 21, 166-175, (1994)
37. Heaney, P. J., Reviews in Mineralogy, Mineralogical Society of America, Washington, D.C., 29, 1-40, (1994).
38. H. Graetsch and O. W. Florke, Zeitschrift fur Kristallographie, 195, 31-48, (1991).
39. JCPDS-ICDDNo.48-0652
40. JCPDS-ICDD No.31-0028
41. JCPDS-ICDD No.42-1401
42. JCPDS-ICDD No.39-1425
43. De Pablo-Galan, M., et al. *Phys. Chem. Min.* **24** 90-101 (1997).
44. Guthrie, George D. Jr., Bish, David L., and Reynolds, Robert C, Jr. "Modeling the x-ray diffraction pattern of opal-CT" *Am. Min.* 80, 869-872, (1995).

45. M. Y. Xu, H. Jain, M. R. Notis, American Mineralogist, 74, 821-825, (1989).
46. F. Bartoli, D. Bittencourt-Rosa, M. Doirisse, R. Meyer, R. Philippy, J. Samama, Eur. J. Mineral., 2, 611-619, (1990).
47. S. Daviero, C. Avinens, A. Ibanez, J.C. Giuntini, and E Philippot, Journal of Non-Crystalline Solids, 146, 279-284, (1992).
48. M. Rokita, M. Handke, and W. Mozgawa, Journal of Molecular Structure, 511-512, 277-280, (1999).
49. J. Wong, Journal of Non-Crystalline Solids, 20, 83-100, (1976).
50. M. D'Apuzzo, A. Aronne, S. Esposito, and P. Pernice, Journal of Sol-Gel Science and Technology, 17, 247-254, (2000).
51. F. Pechar, Crystal Res. and Technol., 20(2), 239-246, (1985).
52. A. Ortiz, J.C. Alonso, v. Pankov, A. Huanosta, E. Andrade, Thin Solid Films, 368, 74-79, (2000).
53. J. M. Durand, A. Ibanez, A. Goiffon, and E. Philippot, Journal of Solid State Chemistry, 109, 106-111, (1994).
54. S. B. Rice, H. Freund, W. L. Huang, J. A. Clause, C. M. Isaacs, Journal of Sedimentary Research, A65(4), 639-647, (1995).
55. Carmen N. Afonso, Simon Capecchi, Henk der Waal, Anne Jans Faber, Stefano Pelli, Giancarlo C. Righini, Alessandro Verciani and Yingchao Yan, "Erbium-Doped Glass Waveguides for Integrated Optical Amplifiers and Lasers," *SPIE,* **3211**, 341-346, 1997.
56. Michele A. Forastiere, Massimo Guglielmi, Alessandro Martucci and Giancarlo C. Righini, "Rare-Earth-Doped Sol-Gel Waveguides: A Review," *SPIE,* **3280**, 57-66, 1998.
57. Rogojan, R., Sterian, P. E., and Elisa, M. "Aluminophosphate-doped glasses with rare-earch ions." *SPIE* **4068**, 90-96 (2000).
58. Strohhofer, C., Fick, J., Vasconcelos, H.C., and Almedia, R.M. "Active optical properties of Er-containing crystallites in sol-gel derived glass films." *J. Non-Cryst. Solids* **226** 182-191 (1998).

Appendix A
TEM micrographs

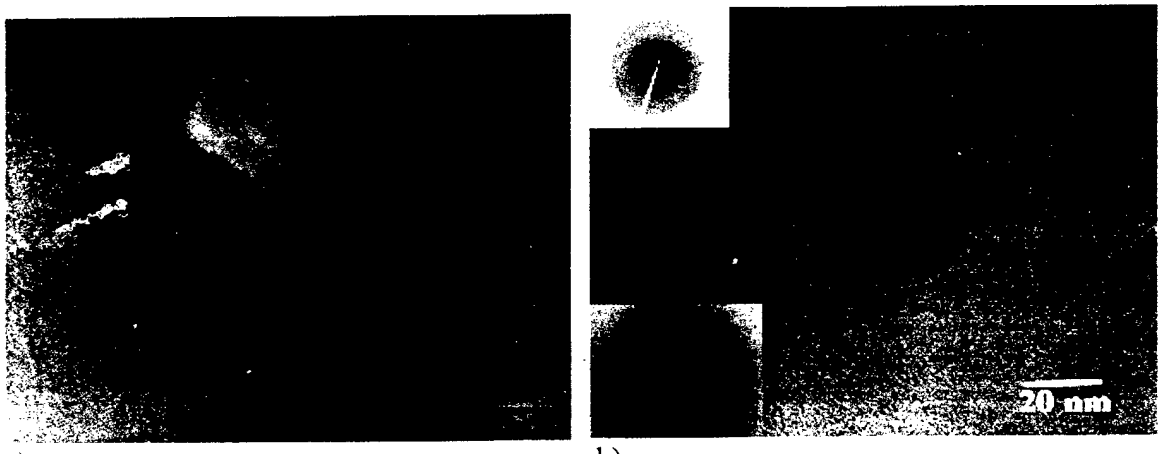

a) b)

Figure A1. Micrographs of Cerablak (x=0.75) annealed at 1100°C, 1h. a) nanocrystalline inclusion b) inclusion with electron diffraction patterns from the amorphous matrix (top) and nanocrystalline inclusion (bottom).

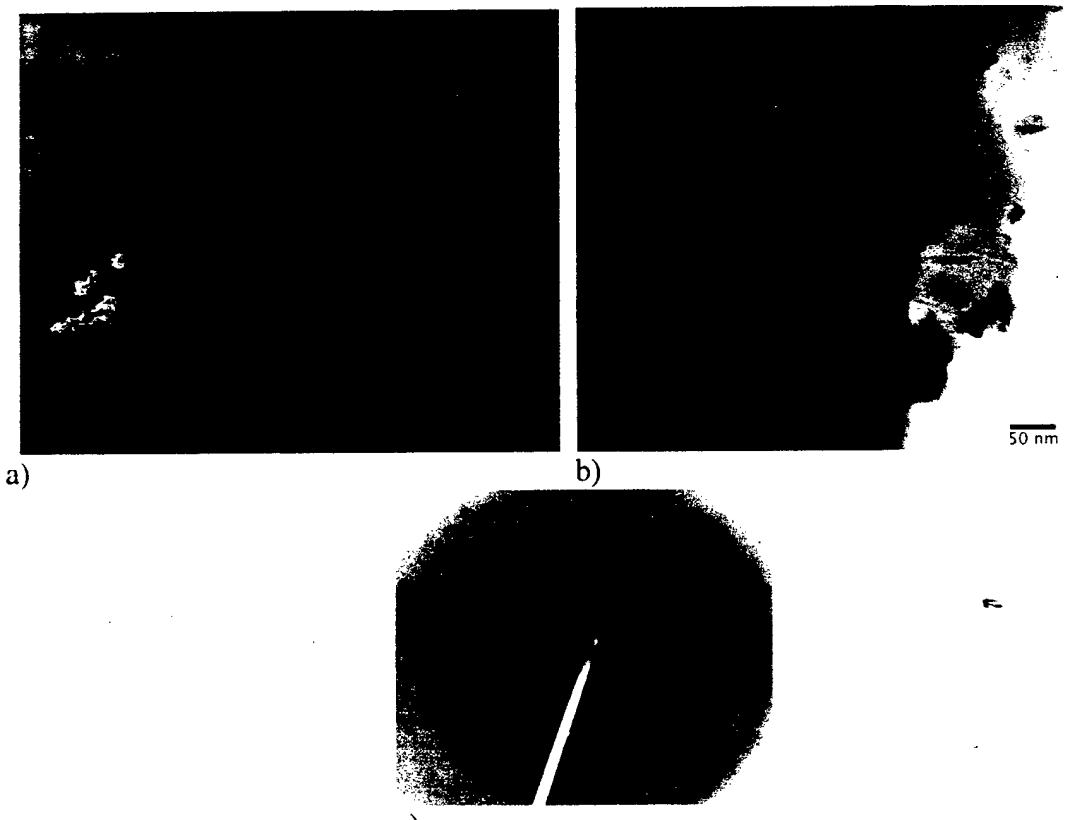

a) b)

c)

Figure A2. TEM micrographs of Cerablak (x=0.75) annealed to 1200°C, 420h. a)bright field micrograph b) dark field micrograph c) electron diffraction pattern of nanocrystalline inclusion and amorphous matrix.

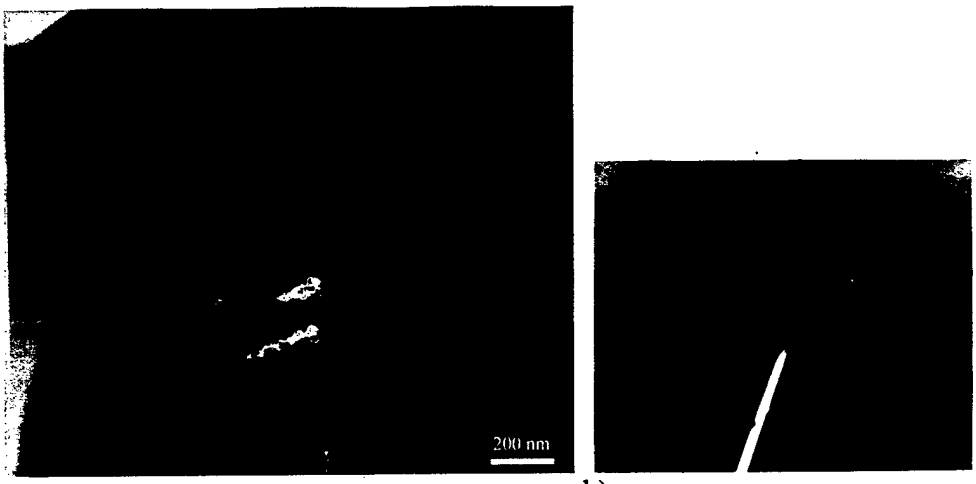

a) b)

Figure A3. a) TEM micrograph of Cerablak (x=0) annealed 1200°C/420hr b)electron diffraction pattern of nanocrystalline inclusion in amorphous matrix.

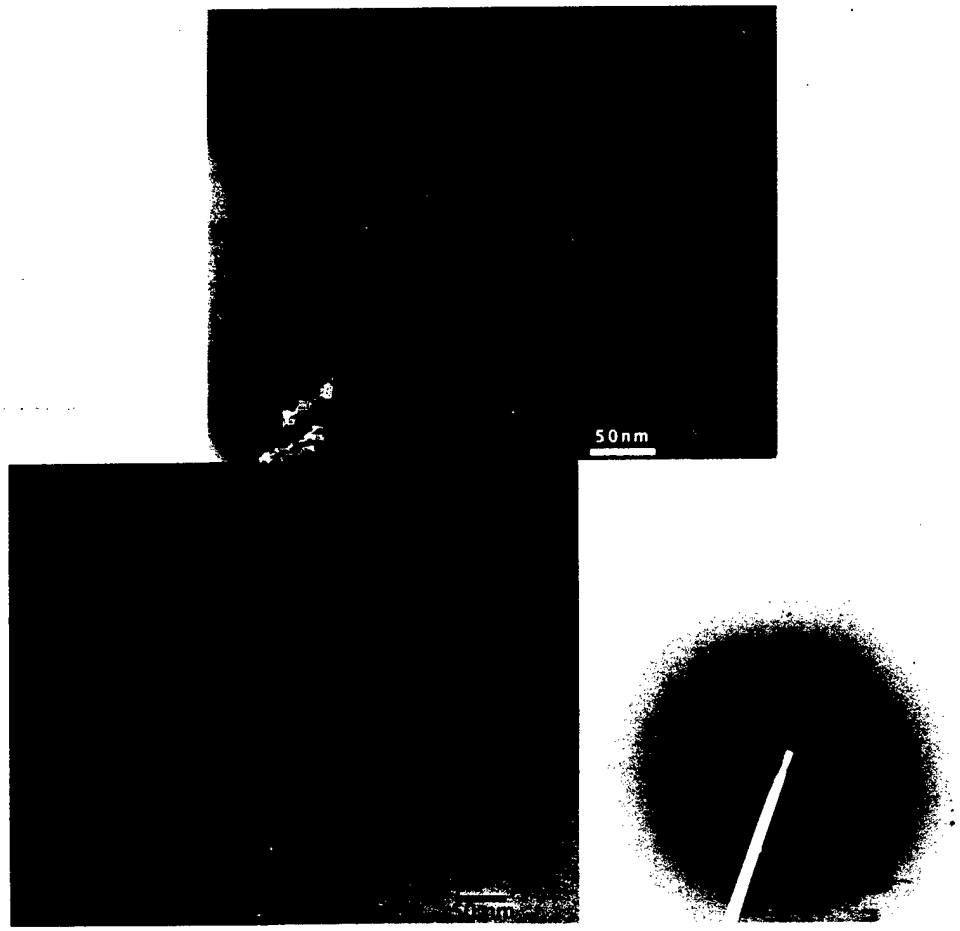

Figure A4. TEM micrographs of Cerablak (x=0.75) annealed 1300°C, 100h, with electron diffraction pattern of nanocrystalline inclusion embedded in amorphous matrix.

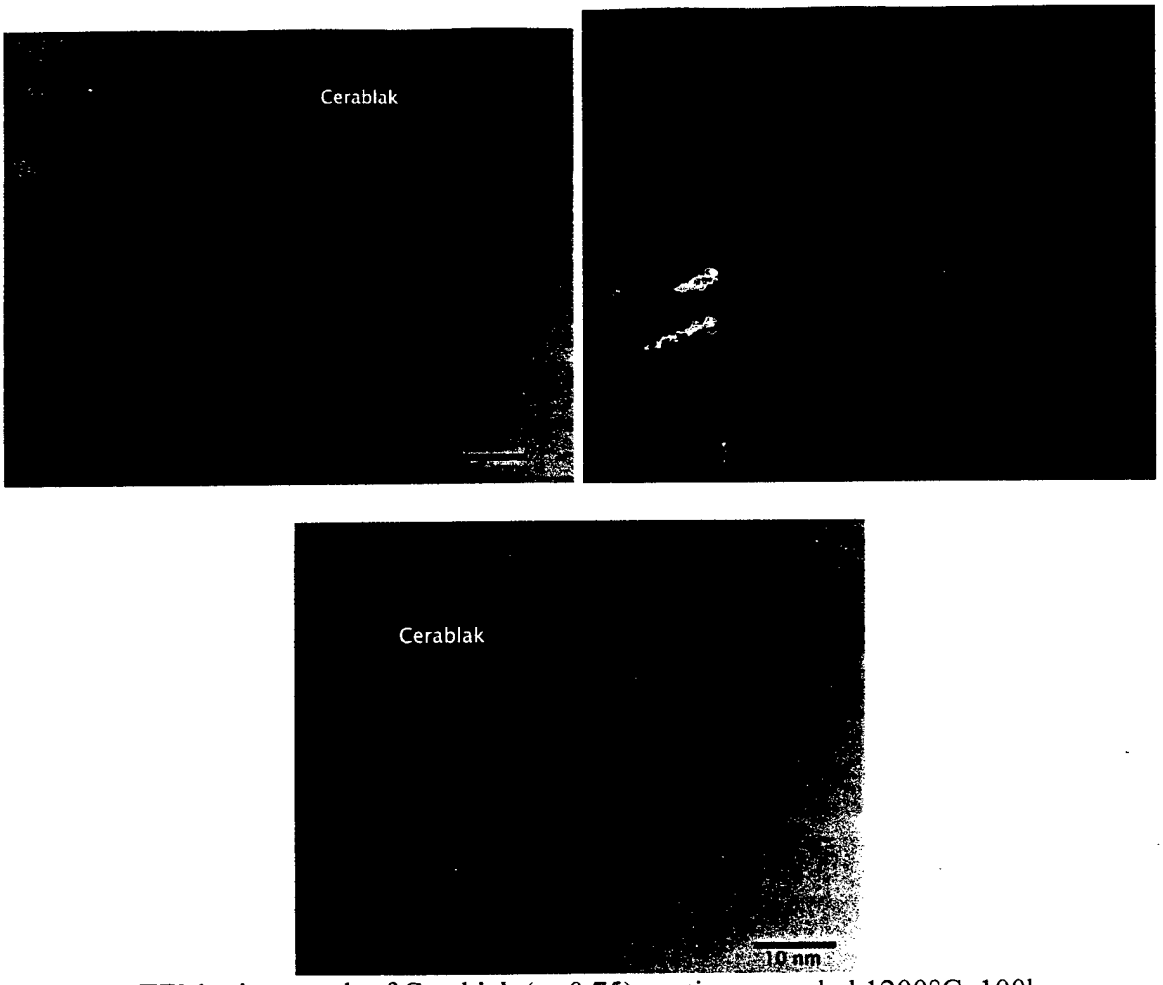

Figure A5. TEM micrograph of Cerablak (x=0.75) coating annealed 1200°C, 100h.

Appendix B

Spectroscopic Data

Raman Spectra

Table BI. Sample identification for Raman samples

Sample number	Composition (x=)	Anneal schedule	Color
S1	berlinite		white
S2	berlinite		white
S3	0.75	1400 °C/ 1hr	
S4	0.75	1100 °C/ 163hr	white/black
S5	0.75	1100 °C/ 1hr	black
S6	0.75	1300 °C/ 100hr	black
S7	0.75	1400 °C/ 10hr	black
S8	0.75	1200 °C/ 100hr	black
S9	0	1100 °C/ 100hr	black
S10	0	1100 °C/ 1hr	black
S11	0	1400 °C/ 36hr	white
S12	9	1100 °C/ 100hr	white

Conventional Laser Raman Scattering experimental details:
Laser excitation wavelength 514.531 nm
Laser power: <0.35 milliWatts at sample unless otherwise noted
Spectral region: 120-2200 cm^{-1}
Micro Raman backscattering configuration (50 X Mititoya objective)
Spatial resolution < 5 microns
Polarization: All spectra are HV depolarized unless otherwise noted

Notes on Raman Spectra:
The polarized/depolarized Raman spectra of S5 clearly display bands that can be associated with an amorphous network.

The 1350 and 1600 cm^{-1} bands disappear if the laser intensity is set too high. Both bands disappear together. In all of the Raman spectra, these bands always appear together and only on black grains. The intensity of these bands decreases with increasing annealing temperature and time.

Depolarized (HV) Raman spectra in the region between 2000 and 3800 cm^{-1} were also obtained on sample S5 (Cerablak). Bands in the O-H stretch region were extremely weak, barely above background noise level. At a power level of 0.34 mW, a broad feature at 2950 cm^{-1} was observed with an intensity of about 4 counts above background. Compare this to Plot 6. The 1600 cm^{-1} band for S5 is approximately 80 cts above background for the same laser power. In pure water, the H_2O bending vibration appears near 1640 cm^{-1} and is considerably *weaker* than the O-H stretching modes. In the CBLK samples, the 1600 cm^{-1} band appears much too intense to be associated with the H_2O bending vibration, although it is

possible that there could be a resonance Raman enhancement of this band in the Cerablak-type materials.

Polarized (VV) Raman spectra in the O-H stretching region were not helpful since they were swamped with a rising fluorescence tail.

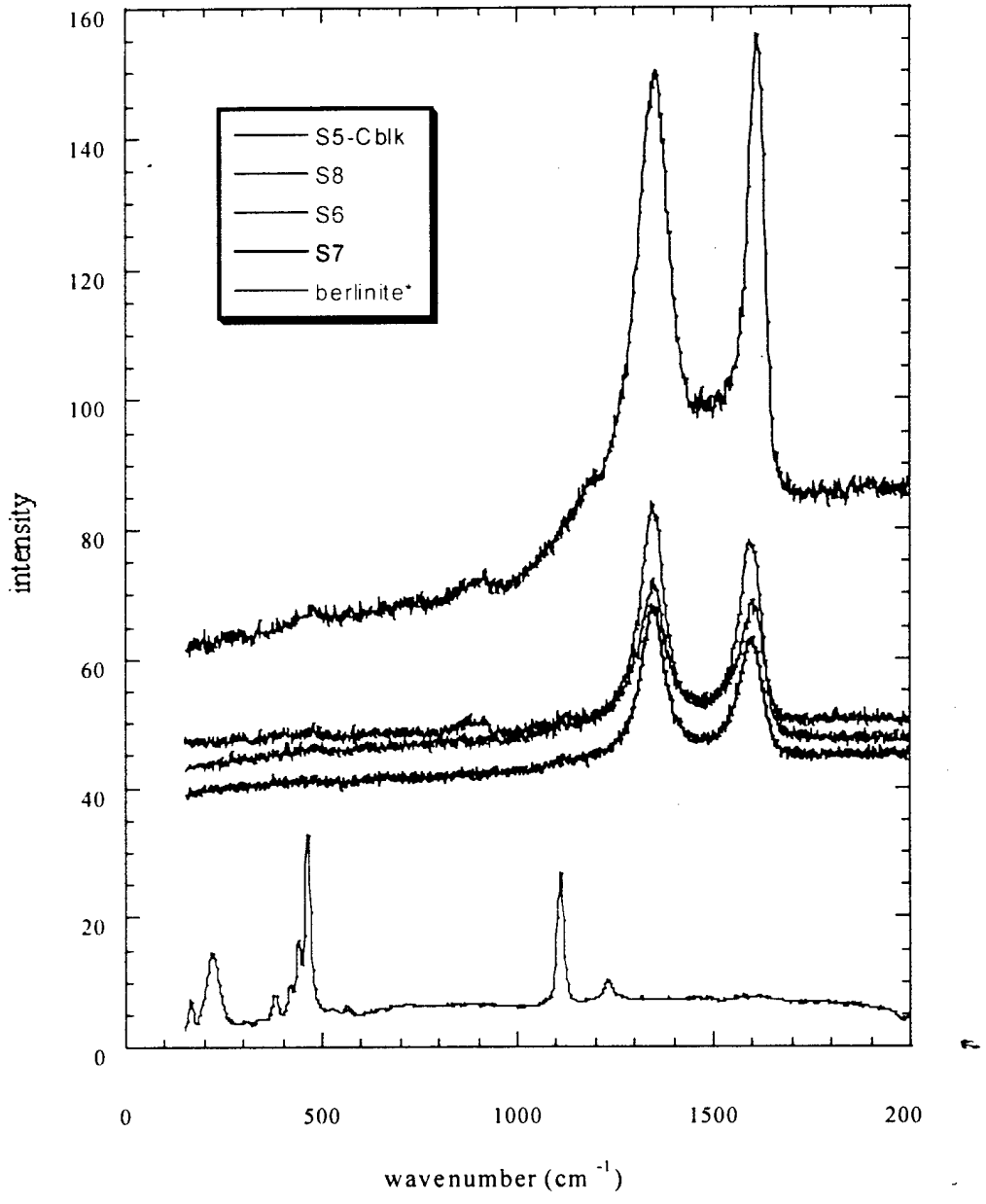

Figure B1. A composite of spectra of all of the samples.

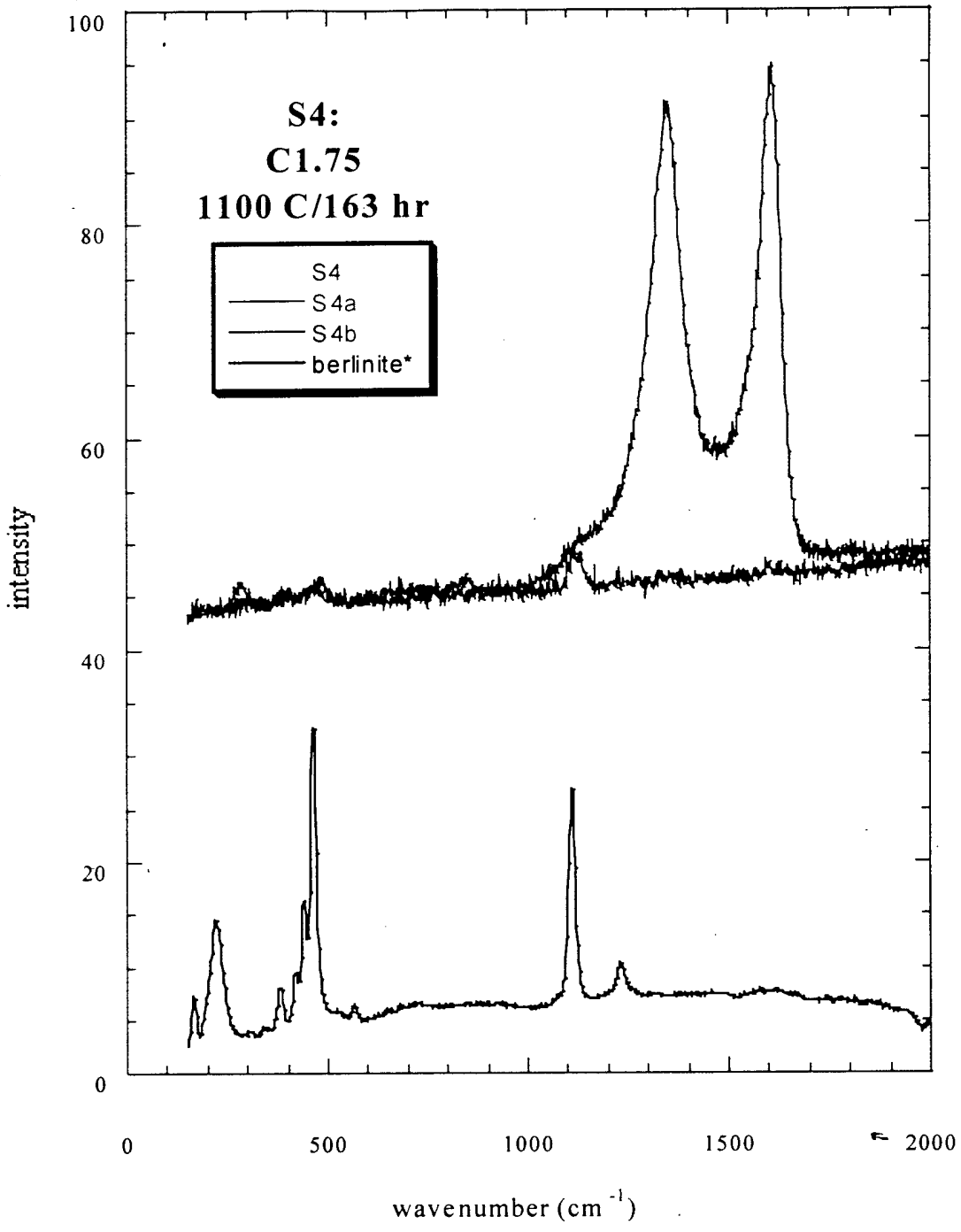

Figure B2. Composite Spectra of Cerablak (S5), S6, S7 and S8.
Comparison spectrum of berlinite is also shown. These samples all show very prominent bands at 1350 and 1600 cm^{-1}. The samples were generally homogeneous.

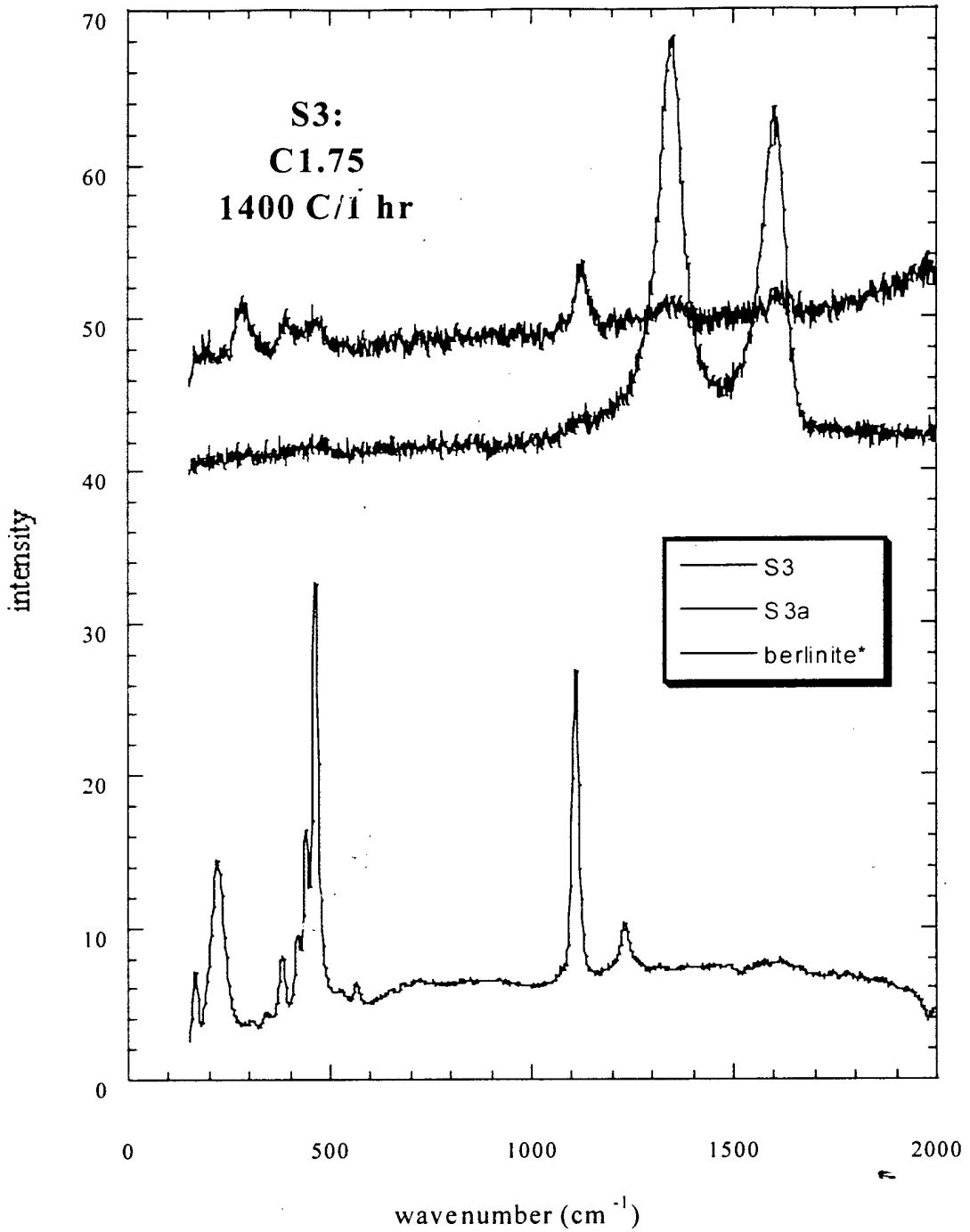

Figure B3. Raman spectra of S4 and comparison with berlinite.
The sample was heterogeneous comprised of a light colored fine grained matrix and imbedded black grains. The matrix material exhibits $AlPO_4$ crystallization without P=O and H_2O bands. The dark material is amorphous and displays the usual 1350 and 1600 cm^{-1} bands.

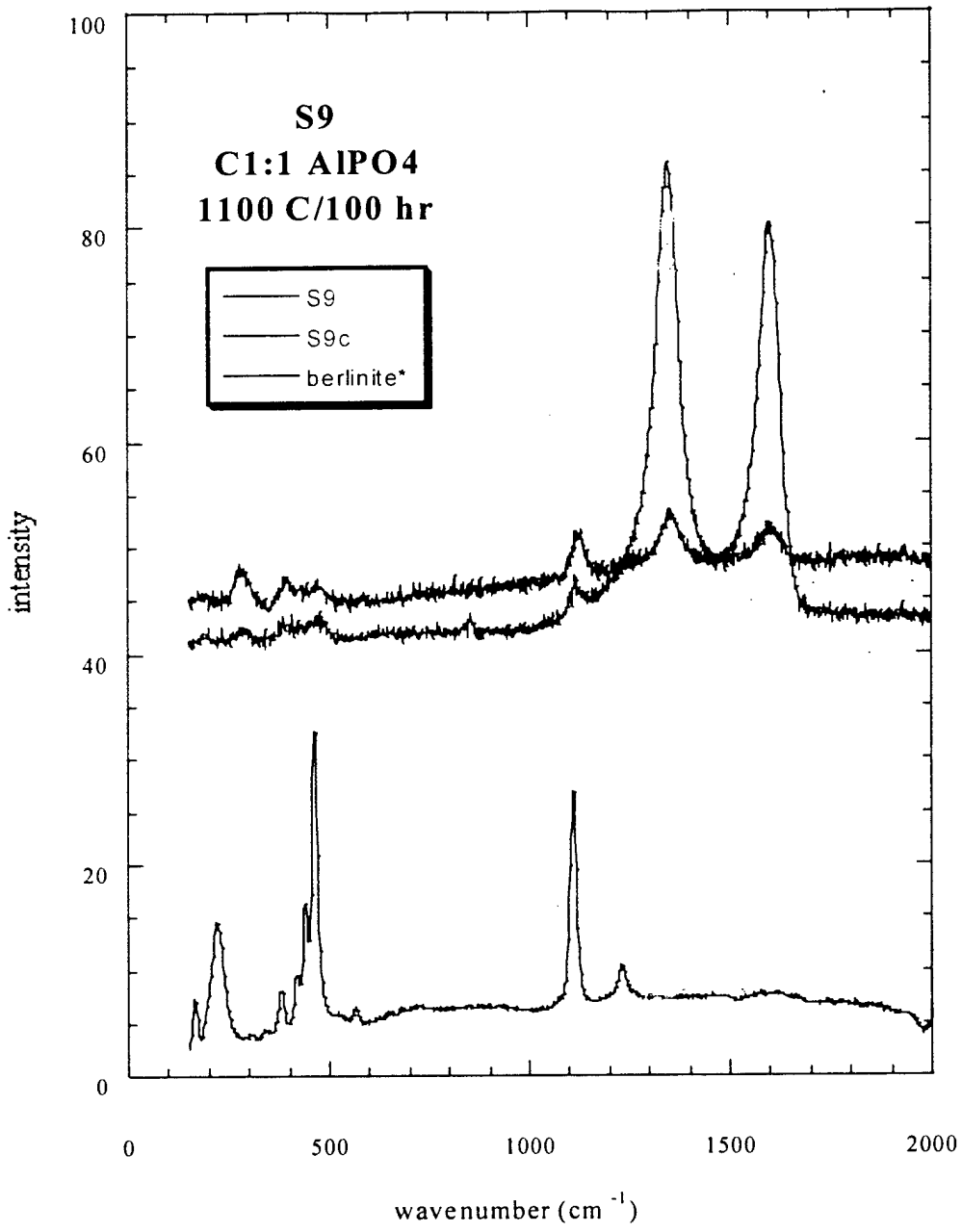

Figure B4. Raman spectra of S3 and comparison with berlinite.
The sample was heterogeneous comprised of a light colored fine grained matrix and imbedded black grains. The matrix material exhibits $AlPO_4$ crystallization without P=O and H_2O bands. The dark material is amorphous and displays the usual 1350 and 1600 cm^{-1} bands.

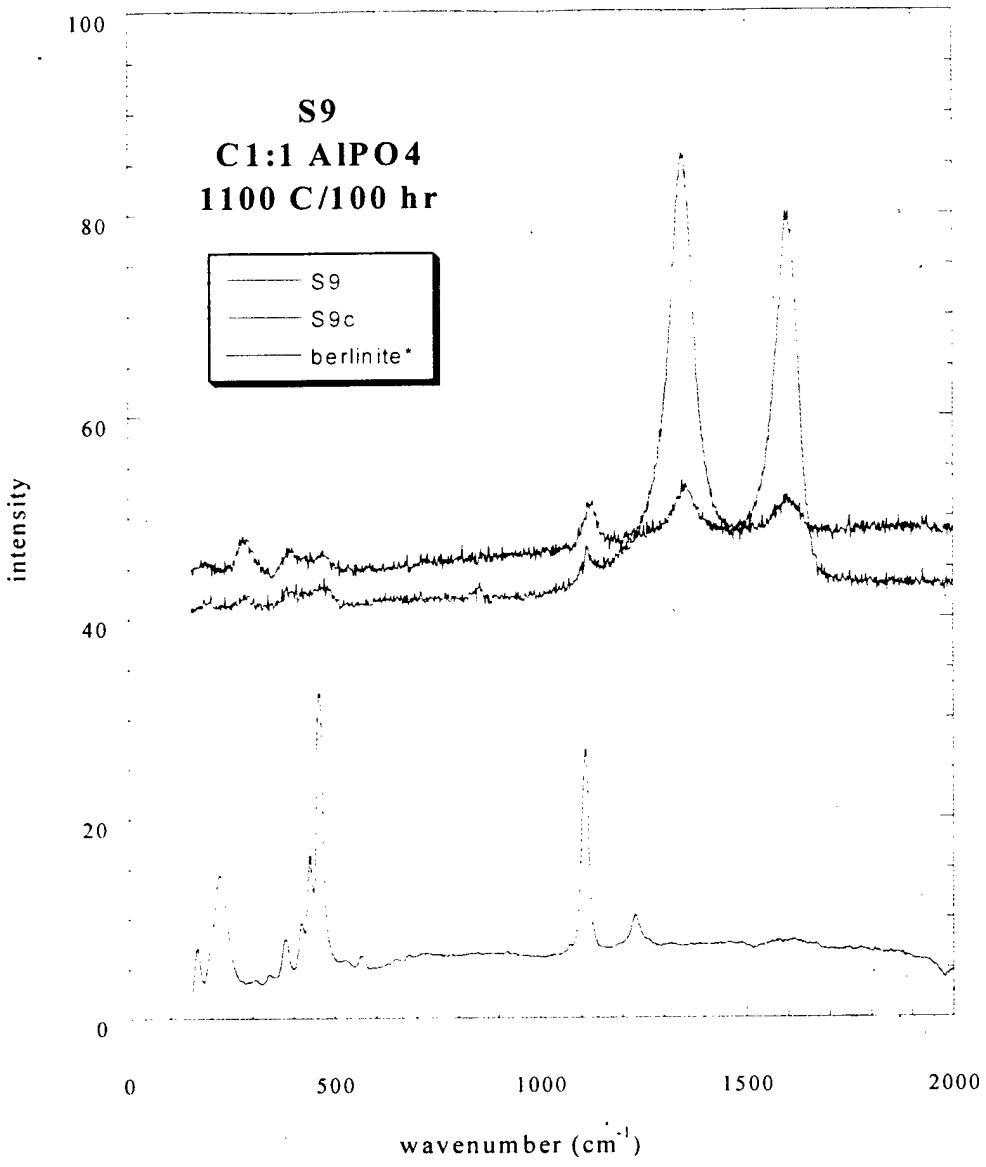

Figure B5. Raman spectra of S9 and comparison with berlinite.
The sample was heterogeneous comprised of a light colored fine grained matrix and imbedded black grains. The matrix material exhibits $AlPO_4$ crystallization without P=O and H_2O bands. The dark material is amorphous and displays the usual 1350 and 1600 cm^{-1} bands.

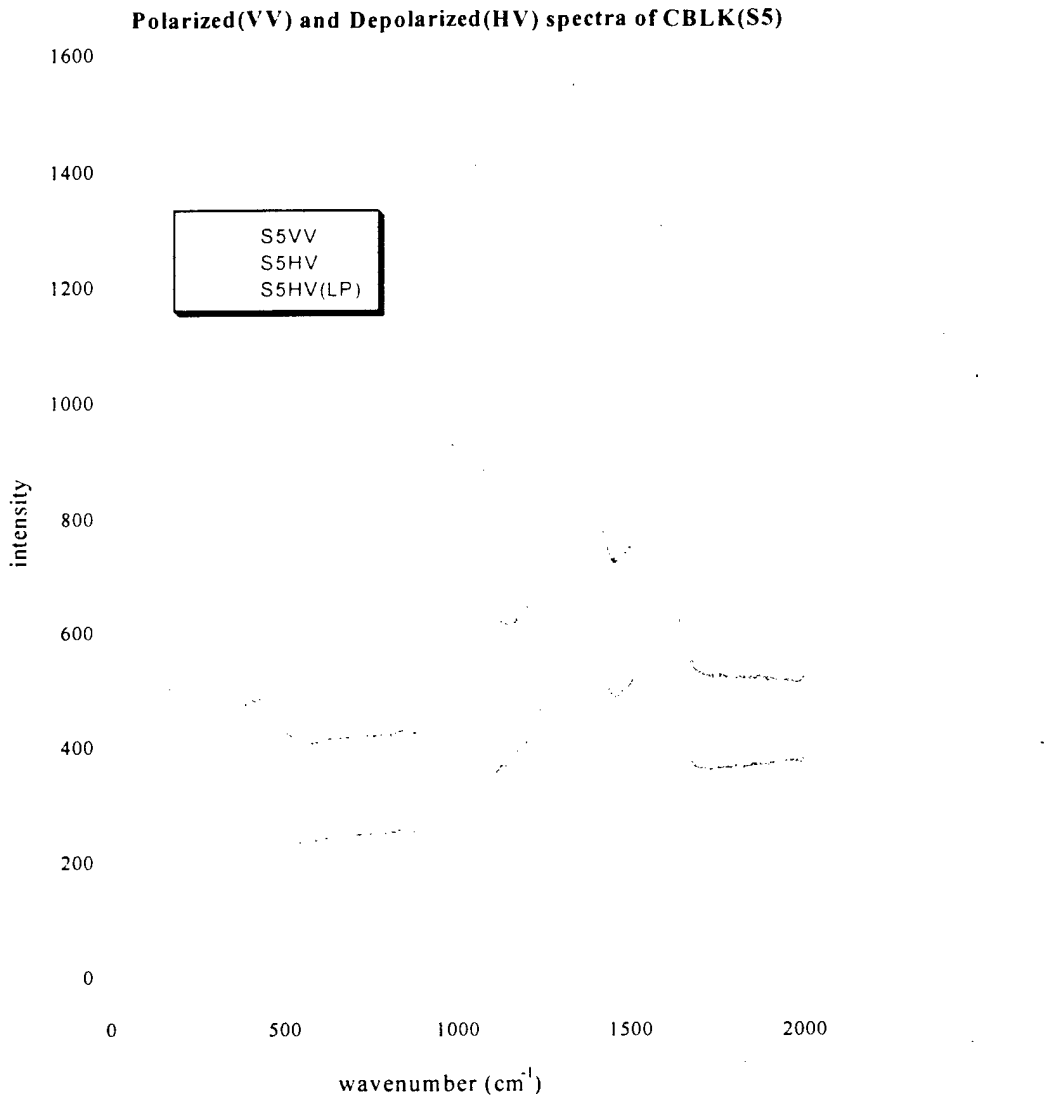

Figure B6. Comparison of the Polarized (VV) and Depolarized (HV) Raman spectrum of Cerablak sample (S5).

S5vv: It is a higher power VV polarized spectrum (about 4.5 mW at sample. The spectrum is quite nice. In addition to the high frequency bands above 1300 cm-1, it also shows the Raman bands for the amorphous framework: bands at 272, 450, 840 and 1118 cm^{-1}. Note that the high frequency bands have been shifted down to 1336 and 1585 cm^{-1} due to heating under the laser beam. At lower powers (no heating), these peaks appear at 1350 and 1610 (nominal).

S5hv: HV depolarized spectrum of Cerablak. Laser power about 3.6 mW at sample. Note that the amorphous framework Raman bands are much weaker in the depolarized spectrum (as they should be). The high frequency bands are at 1340 and 1588 cm^{-1} and remain intense with this polarization.

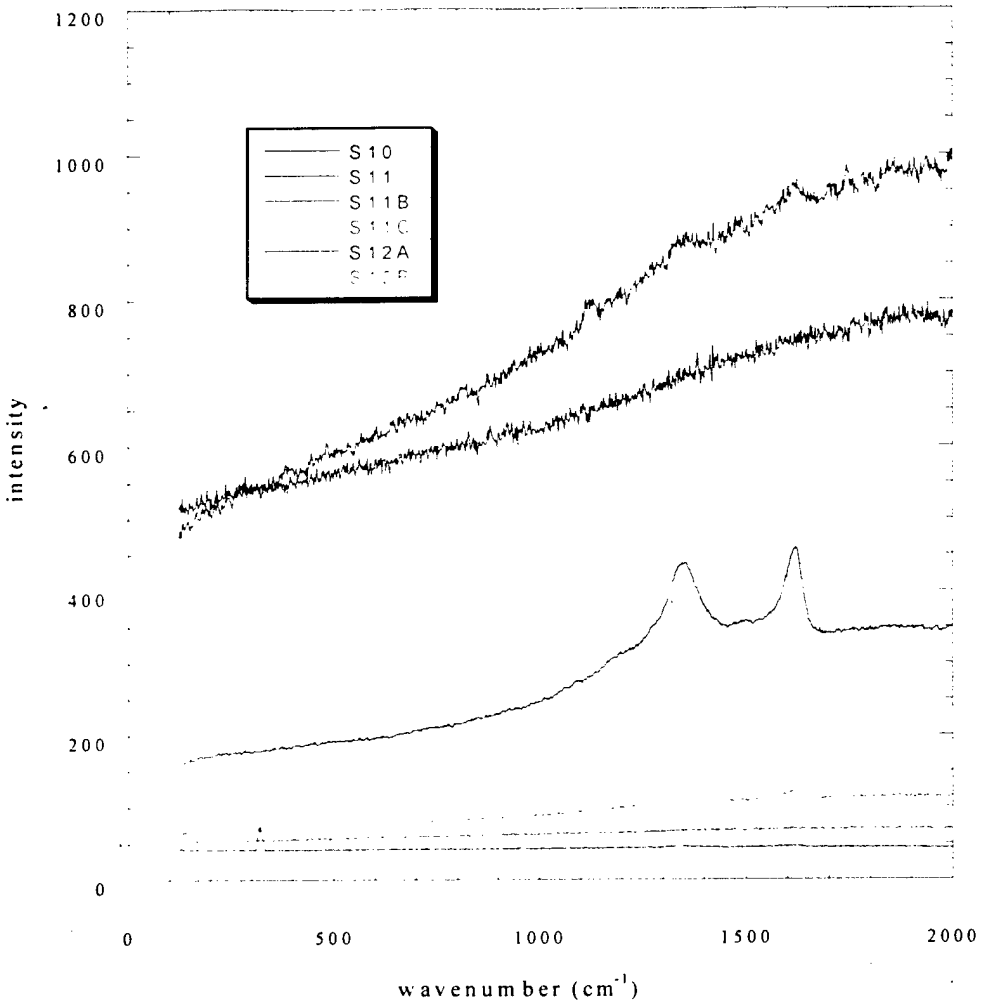

Figure B7. Raman spectra of S10, S11 and S12.
Sample S10 was black and generally homogeneous. Samples S11 and S12 were predominantly white, with very fine grained black grains (< 1 micron size). Sometimes these black grains were clustered.
Spectra from the white matrix are labeled by S11 and S12A. The white matrix material does not show the 1350 and 1600 cm^{-1} bands (some weak residual bands in this region are sometimes observed due to the presence of very tiny black grains).

S11A, S12B and S12C are from regions that contain the small fine grained black material. These regions are predominantly white but with a higher density of black grains. Weak bands at 1350 and 1600 cm^{-1} are observed. These spectral features are likely associated with the dark grains. (Figure B8 gives an exploded view of these weak Raman spectra.)

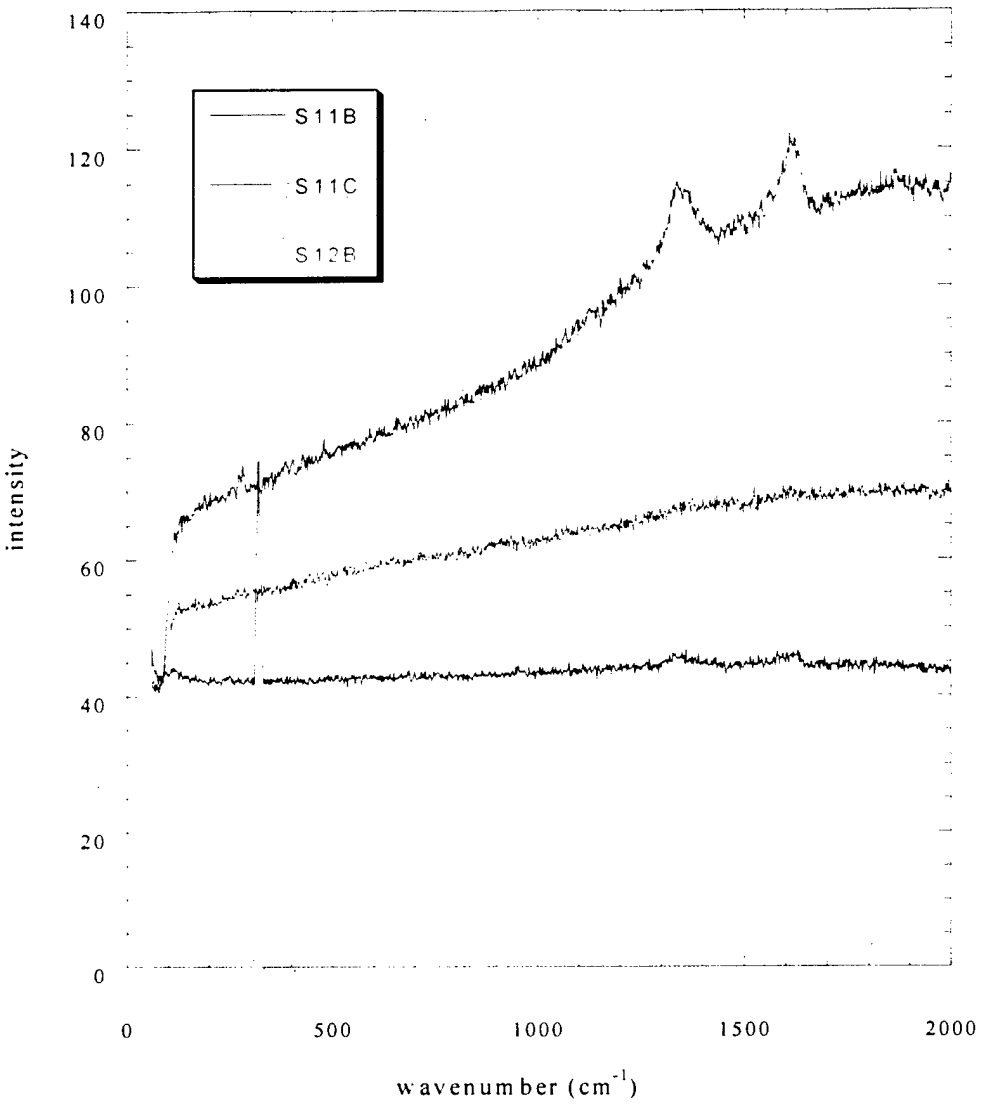

Figure B8. Magnified intensity display of the Raman spectra for S11A, S12B and S12C. Weak bands at 1350 and 1600 cm^{-1} are observed. These spectral features are likely associated with the dark grains.

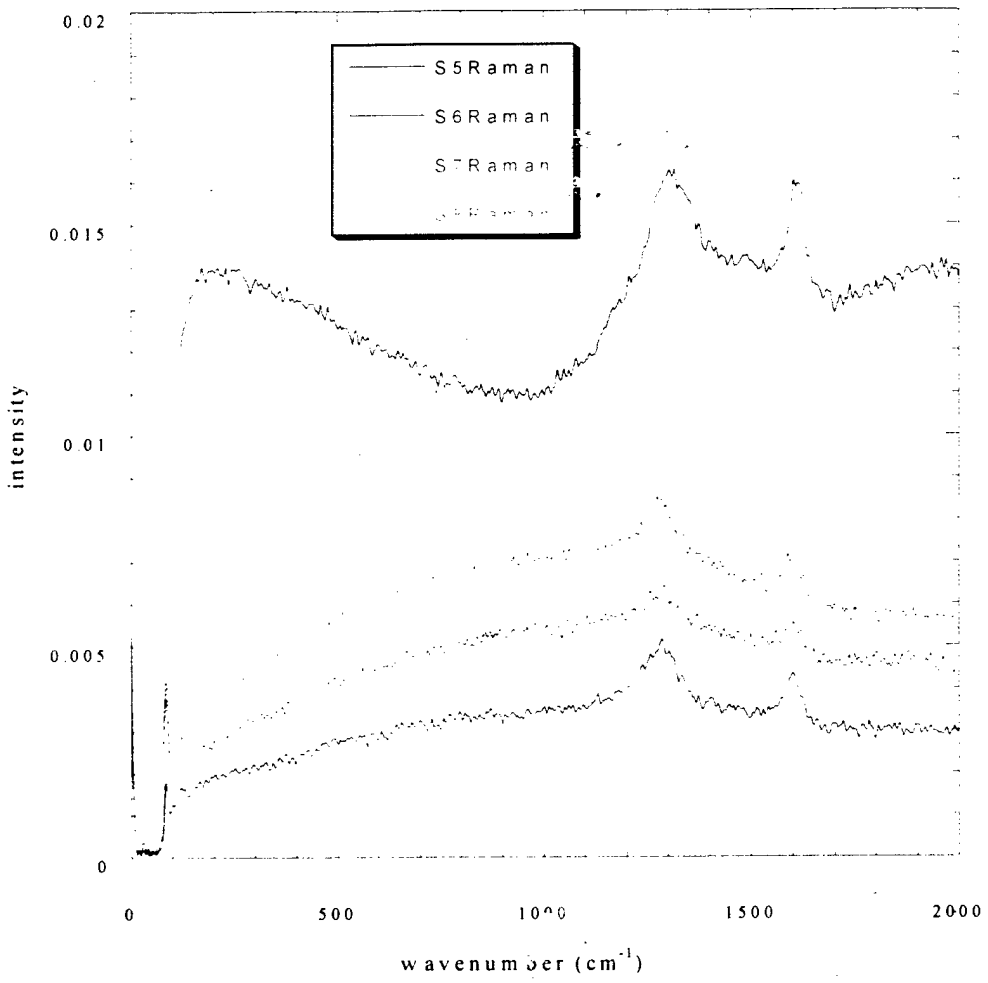

Figure B9. FTRaman Spectra of samples S5, S6, S7, and S8.
Laser excitation here is 100 mW at 1064 nm. The beam is unfocused with a spot size of about 0.5 mm. For the S5 sample, the intense high frequency bands appear at 1313 and 1613 cm^{-1}. For the conventional Raman spectra shown in Plot 6, the corresponding bands appear at 1350 and 1610 cm^{-1} at low laser power (0.34 mW/focused), and 1336 and 1585 cm^{-1} for high laser power (4.5 mW/focused).

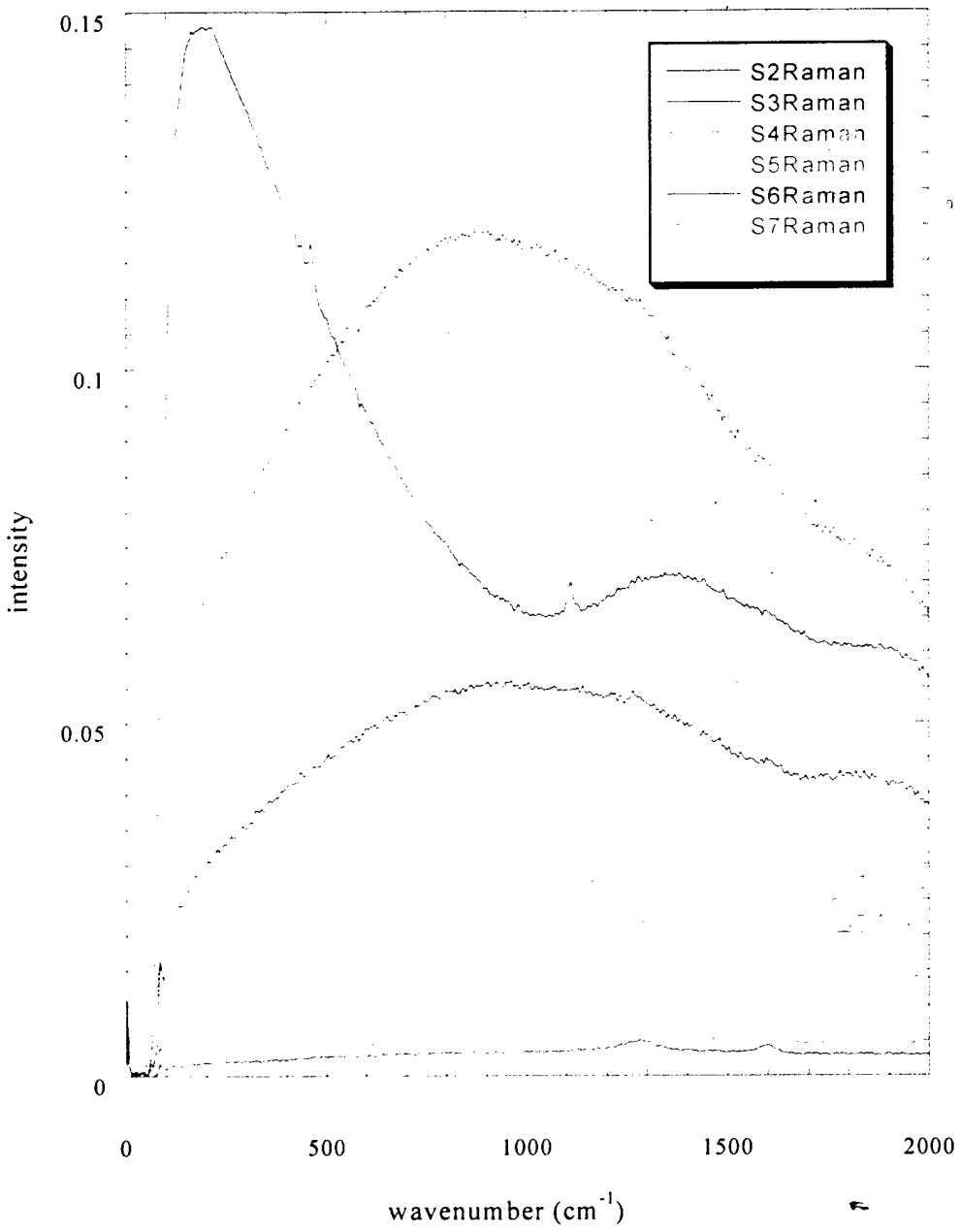

Figure B10. Compilation of the FTRaman Spectra of samples S2-S8.

FTIR Spectra

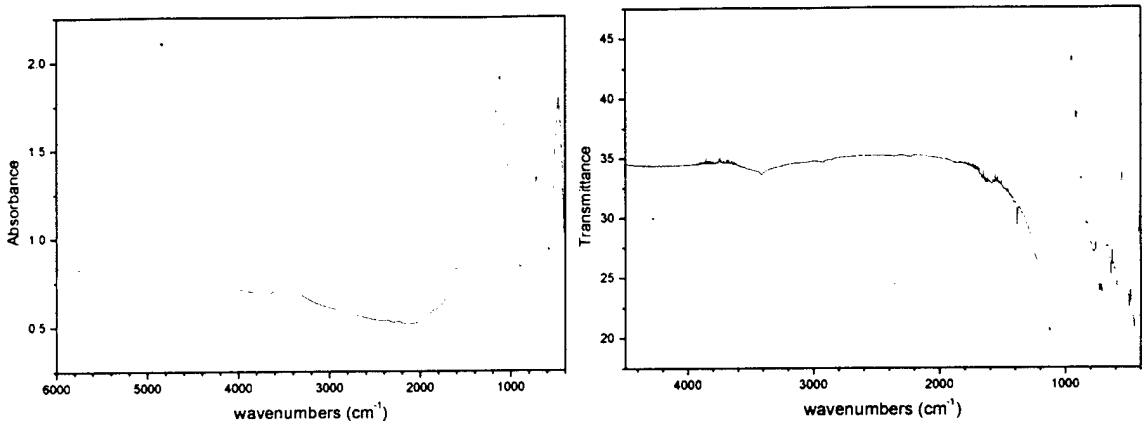

a) b)

Figure B11. Cerablak (x=0.75) after anneal at a)1300°C, 100h. b) 1400°C, 10h.

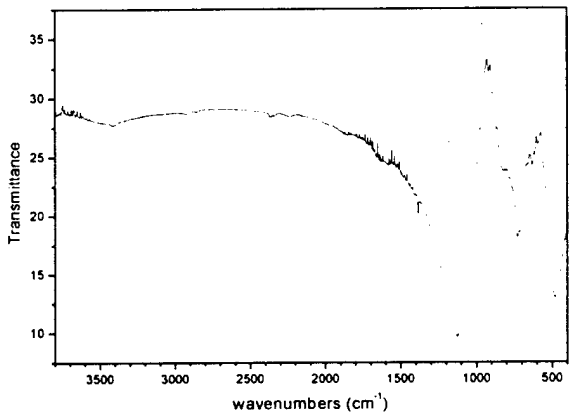

Figure B12. Cerablak (x=0.5) after anneal at 1200°C, 100h.

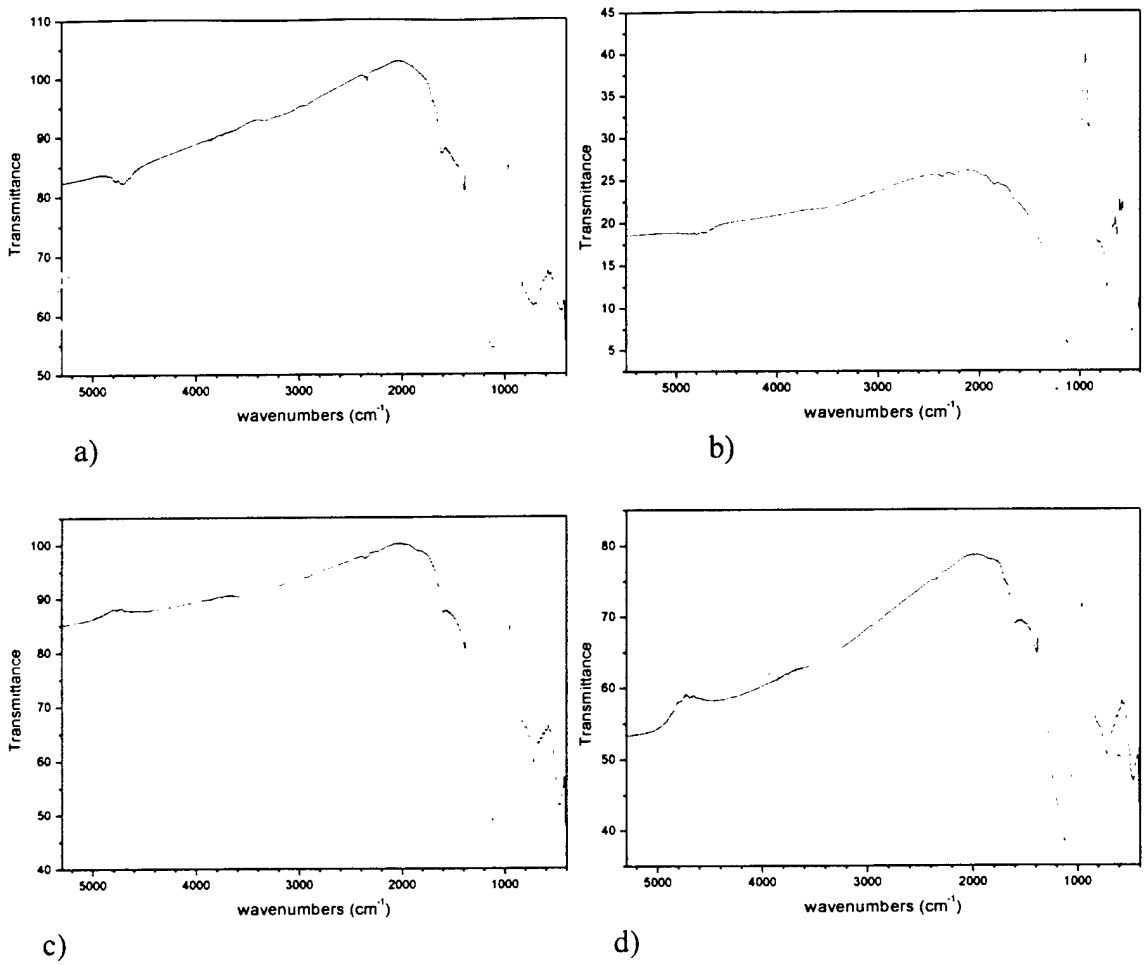

Figure B13. Aged Cerablak (x=0.75) after 1000°C, 0.5hr anneal. a) 21 months old. b) 19 months old. c) 17 months old. d) 15 months old.

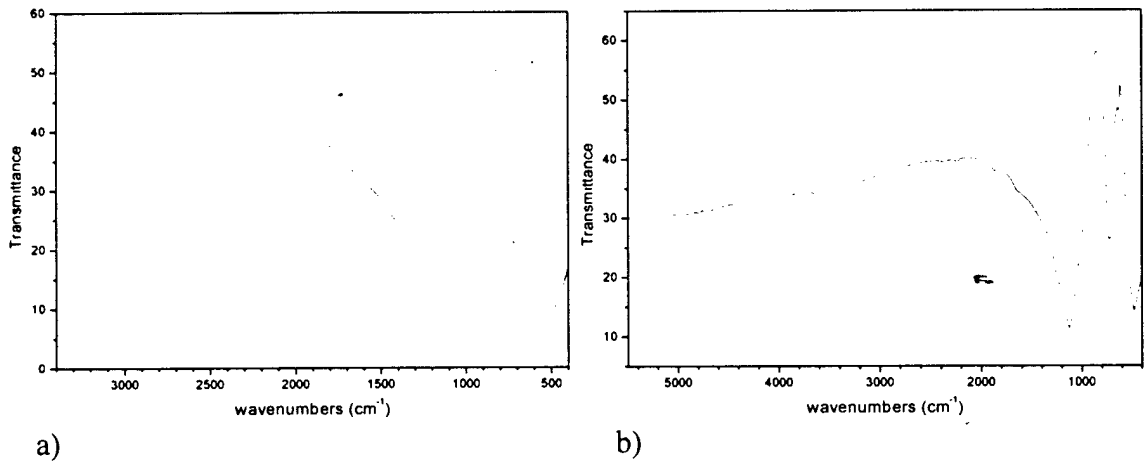

Figure B14. Substoichiometric Cerablak (x=-0.25) after anneal at a)1100°C, 24h. b)1100°C, 163h.

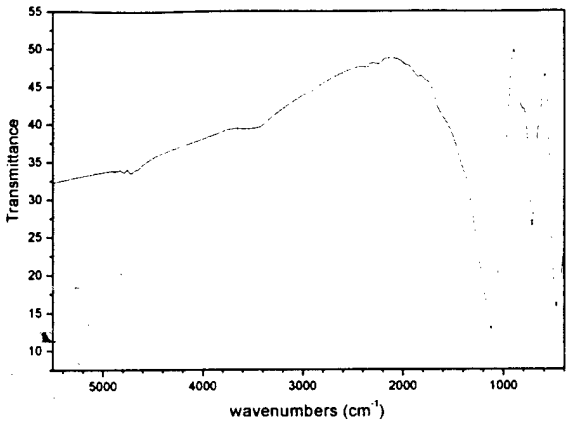

Figure B15. Substoichiometric Cerablak (x=-0.06) after anneal at 1100°C, 24h.